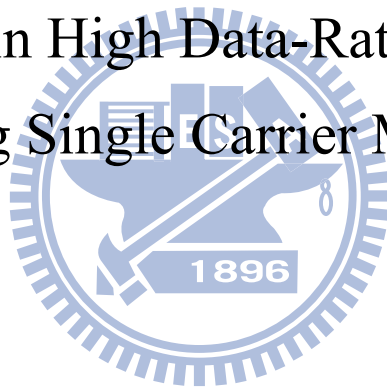# 國 立 交 通 大 學

光 電 工 程 研 究 所

碩 士 論 文

等化器應用於高頻譜效率之單載波

倍頻光載微波信號系統

Equalization in High Data-Rate RoF System

Employing Single Carrier Modulation

研 究 生：何彥霖

指導教授：陳智弘　教授

中 華 民 國 九 十 九 年 六 月

等化器應用於高頻譜效率之單載波
倍頻光載微波信號系統
Equalization in High Data-Rate RoF System
Employing Single Carrier Modulation

研 究 生：何彥霖　　　　　　　Student : Yen-Lin Ho

指導教授：陳智弘　教授　　　　Advisor : Dr. Jyehong Chen

A Thesis

Submitted to Department of Computer and Information Science

College of Electrical Engineering and Computer Science

National Chiao Tung University

in partial Fulfillment of the Requirements

for the Degree of Master in

Department of Photonics

Hsinchu, Taiwan 300, R.O.C

中 華 民 國 九 十 九 年 六 月

Acknowledgements

碩士班這兩年，首先，我要感謝我的指導老師 陳智弘教授，提供良好的實驗環境及器材，以及專業的指導及照顧，讓我在碩士班兩年的生活中有明顯的進步。另外，要感謝林俊廷學長的指導，教導我許多關於實驗操作的方法以及上台報告的方法，由於林俊廷學長的教導，給我正確的觀念與理論。此外，我還要感謝，施伯宗學長，江文智學長，感謝他們在我做實驗時，幫我解決問題和教導我一些做實驗的技巧，以及提供程式上的協助。

接著，我要感謝我的實驗室夥伴。謝謝立穎在碩士兩年的期間幫我不少的忙。另外，也要感謝芳銘學長陪伴我一起度過我的碩士班生活。再來，我要感謝實驗室學弟們，在我實驗忙碌的時候幫忙處理一些瑣事。

最重要的，我要感謝我的家人，爸爸、媽媽、他們的支持和叮嚀，以及不停的照顧，讓我可以不用為其他事情煩惱，順利的完成碩士學位。

參雜汗水和歡笑的碩士班的回憶，在大家的照顧和指導所編織而成，謝謝大家的陪伴和指導，讓我順利完成碩士學位，繼續往人生的下段旅程繼續努力。

何彥霖 于 風城 交大 民國九十九年六月

I

等化器應用於高頻譜效率之單載波倍頻光載微波信號系統

研 究 生: 何彥霖　　　　　　　指導教授: 陳智弘 博士

國立交通大學　電機資訊學院

光電工程研究所

摘要

所提出的架構證實為長程 60G 赫茲光纖擷取系統可行的方法。在此架構中，我們使用倍頻的單邊帶調變技術示範一個 60G 赫茲頻段的系統。符號率每秒 2G 的單邊帶單載子 QPSK 訊號以及符號率每秒 2G 的雙邊帶單載子 QPSK 訊號被用來當作下行的訊號。由於修正型 Tandem 單邊帶調變技術的關係，沒有色散所造成之訊號時強時弱的狀況發生，高頻譜響應的向量訊號可被使用。另外由於使用了單邊帶調變技術，因此我們可獲得高於傳統雙邊帶調變技術兩倍的頻譜使用效率。

經過 50 公里的單模光纖傳輸，所試驗的訊號在接收端的能量沒有明顯的損耗。此外，經過等化器對系統頻率響應不佳的補償後，訊號的品質有顯著的改善。

Equalization in High Data-Rate RoF System Employing Single Carrier Modulation

Student: Yen-Lin Ho   Advisor: Dr. Jyehong Chen

Department of Photonics and Institute of Electro-Optical

Engineering,

National Chiao Tung University

ABSTRACT

The proposed scheme proves to be a viable solution for long-reach 60-GHz RoF system. In the scheme, we demonstrate a 60-GHz band radio-over-fiber (RoF) system using a modified tandem single sideband (TSSB) modulation scheme with frequency doubling. Single sideband from Hilbert transform and traditional double sideband single carrier QPSK signal with 2-GBaud symbol rate have been demonstrated to be downlink signal. Because of the modified TSSB modulation scheme, no dispersion induced fading is observed; high spectral efficiency vector signal can be utilized. Because of the single sideband signal we have a better spectrum efficiency.

. After 50km standard single mode fiber (SSMF) transmission, there are no significant receiver power penalty of the demonstrated signals. Besides, there is a significant performance improvement after utilizing an equalizer to compensate un-even system frequency response.

CONTENTS

List of Figures

Chapter 1

Introduction

1.1 Review of Radio-over-fiber system

To achieve the more and more higher data-rate for different kinds of communication application. People develop many applications in the microwave band, such as 3G, WiFi, and WiMAX. These are very important for wireless network.

When the growth of customers or increase data rate led to insufficient bandwidth in microwave band for the users. Hence, to develop higher frequency microwave, even millimeter-wave is an important issue in the future. Due to the higher frequency millimeter-wave signal has smaller coverage area. Hence, we need a lot of base stations to deliver millimeter-wave signal as shown in Fig. 1-1. In order to saving the system cost and less equipped base stations (BSs) along with a highly centralized central station (CS) equipped with optical and mm-wave components are very importance. Using fiber transmission medium is one of the best solutions because there are wider bandwidth and much less power loss in fiber. Therefore, Radio-over-fiber (ROF) systems are attracted and more interesting for potential use in the future. Broadband wireless communications are shown in Fig. 1-2. ROF technology is a promising solution to provide multi-gigabits/sec service because of using millimeter wave band, and it has wide converge and mobility.
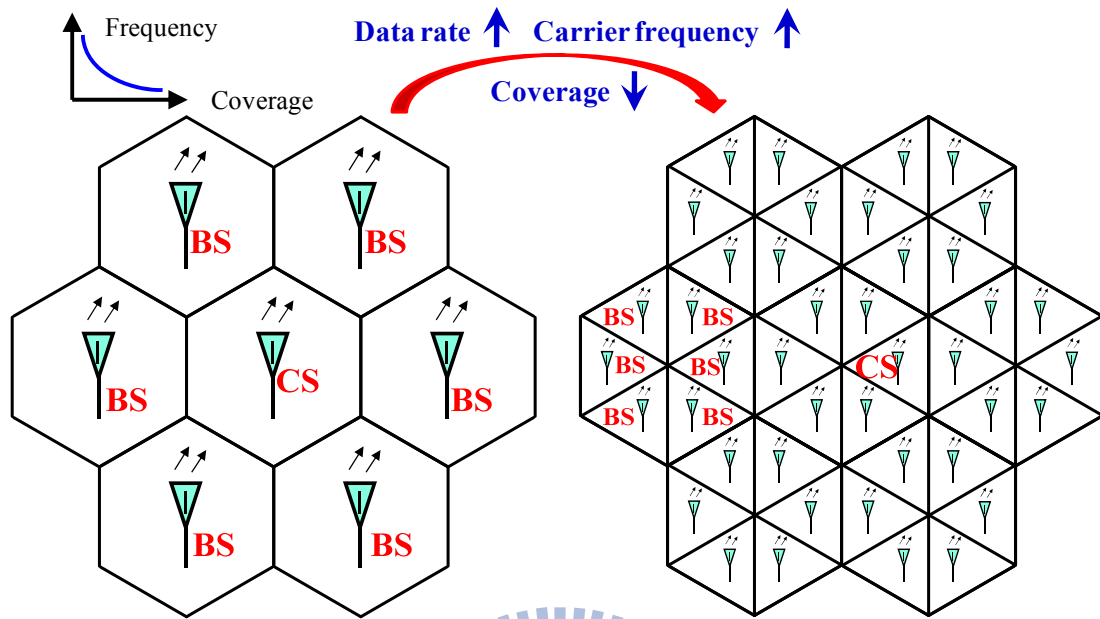
Figure 1-1 Basic structure of microwave/millimeter-wave wireless system
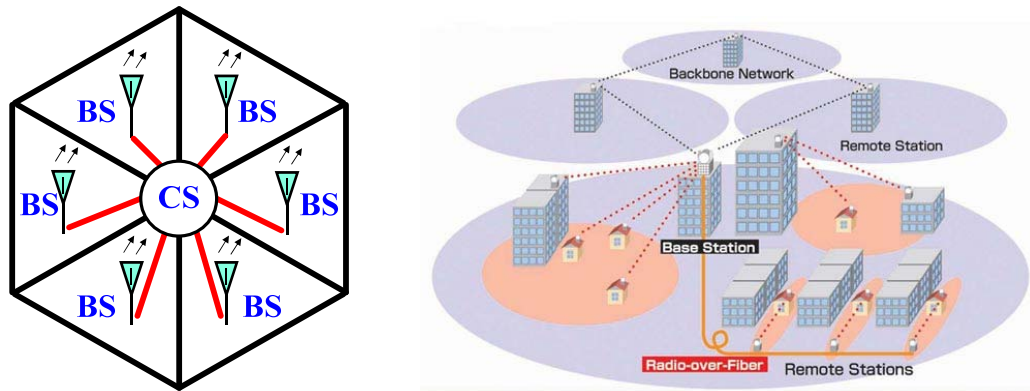
Figure 1-2 the Radio-over fiber system

1.2 Basic modulation schemes

The optical radio frequency (RF) signal generation using an external Mach-Zehnder modulator (MZM) based on double-sideband (DSB), single-sideband (SSB), and double-sideband with optical carrier suppression (DSBCS) modulation schemes have been demonstrated [1,2,4-8]. Since the optical RF signals are weakly modulated because of the narrow linear region of MZM, those that have undergone DSB and SSB modulation suffer from inferior sensitivities due to limited optical modulation index (OMI) [4-6,8]. Hence, an optical filter is needed to improve the performance [8]. Furthermore, the DSB signal experiences the problem of performance fading because of fiber dispersion [6]. Among these modulation schemes, DSBCS modulation has been demonstrated to be effective in the millimeter-wave range with excellent spectral efficiency, a low bandwidth requirement for electrical components, and superior receiver sensitivity following transmission over a long distance [6]. However, all of the proposed DSBCS schemes can only support on-off keying (OOK) format, and none can transmit vector modulation formats, such as phase shift keying (PSK), quadrature amplitude modulation (QAM), or OFDM signals, which are of utmost importance for wireless applications.

On the other hand, optical RF signal generations using remote heterodyne detection (RHD) have been also demonstrated [9-10]. The advantage of RHD systems is that the vector signal can be modulated at baseband. Therefore, the bandwidth requirement of the transmitter is low. However, the drawback is that phase noise and wavelength stability of the lasers at both transmitter and receiver should be carefully controlled.

1.3 Motivation

As wireless communications continues to enjoy phenomenal growth, the ever rising demand for higher data-speeds coupled with the advent of popular bandwidth-hungry applications such as High-Definition (HD) video are putting pressure on wireless communication systems to offer higher data rates. However, data rates of current wireless systems are still limited to several tens of Mbps-hampered by congestion and limited frequency spectrum in their current frequency bands of operation. Since the key to higher data rates is bandwidth, the most promising path to multi-Gbps wireless communication is the use of mm-wave frequencies where very large bands of frequency spectrum are available [11]. For instance, the FCC's 60-GHz band offers 7 GHz of unlicensed spectrum (57-64 GHz). However, mm-wave wireless networking presents many technical challenges owing to the high carrier frequencies and the wide channel bandwidths used [12]–[16]. The challenges include the significantly higher air-link loss (about 30 dB higher at 60 GHz than at 2.4 GHz), and reduced device performance and lower power efficiency. In addition, the wide channel bandwidth means higher noise power and reduced signal-to-noise ratio (SNR). All these factors make wireless networking at 60-GHz "pico-cellular" in nature with the radio cells typically smaller than 10 m. Consequently, multi-gigabit-per-second wireless networking at 60 GHz requires an extensive high-capacity feeder network to interconnect the large number of radio access points.
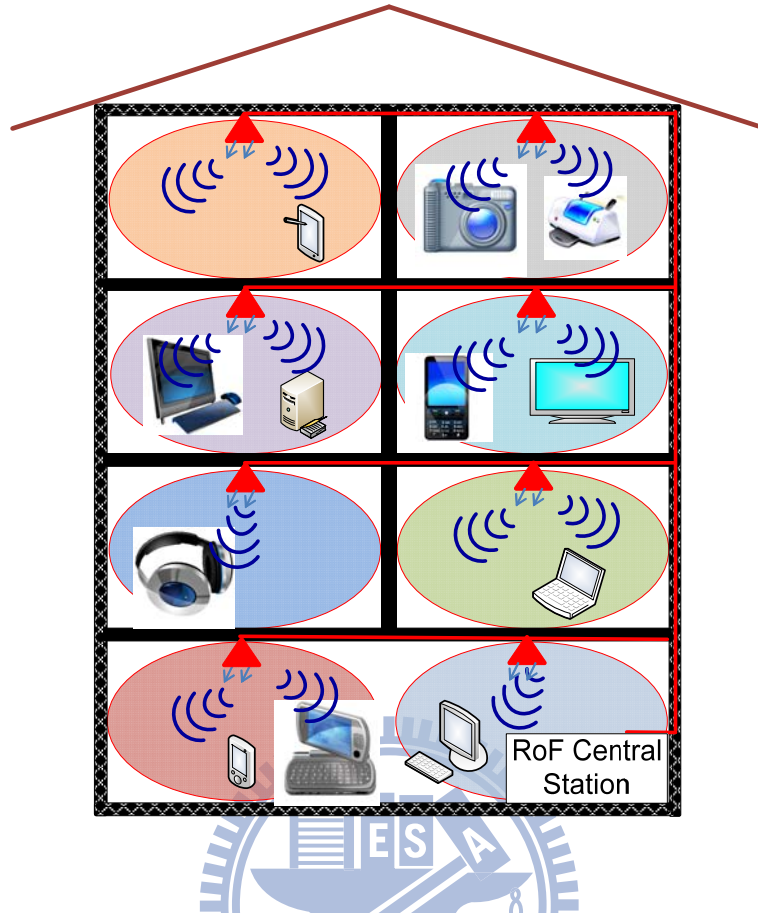
Figure 1-3 Concept of future wireless home network system based on RoF techniques.

Radio-over-Fiber (RoF) technology can provide the required feeder network as it is best suited to deal with the demands of small-cell networks [17]-[19]. A fiber-based Distributed Antenna System (DAS) has the special advantage that it can support the transparent distribution of multiple wireless standards or applications. Figure 1-3 illustrates a cartoon for future 60-GHz wireless home network based on RoF technology. Because of the high path loss and high attenuation through building walls, in-building radio cells at 60 GHz are confined to a single room. This reduces user interference resulting in very high wireless data capacity per user [20].

In order to achieve multi-standard operation, 60-GHz RoF systems must be able to handle wireless signals with different requirements. For instance, for 60-GHz systems, both single-carrier (quadrature amplitude modulation (xQAM)) and multi-carrier (orthogonal frequency-division multiplexing (OFDM)) modulation formats are important. The two formats may impose different system performance requirements on the 60-GHz RoF systems. For instance channel uniformity is very critical for single-carrier systems [21]-[22]. Here we try to use Digital Signal Processing (DSP) to compensate the un-even frequency response and therefore increase signal performance.
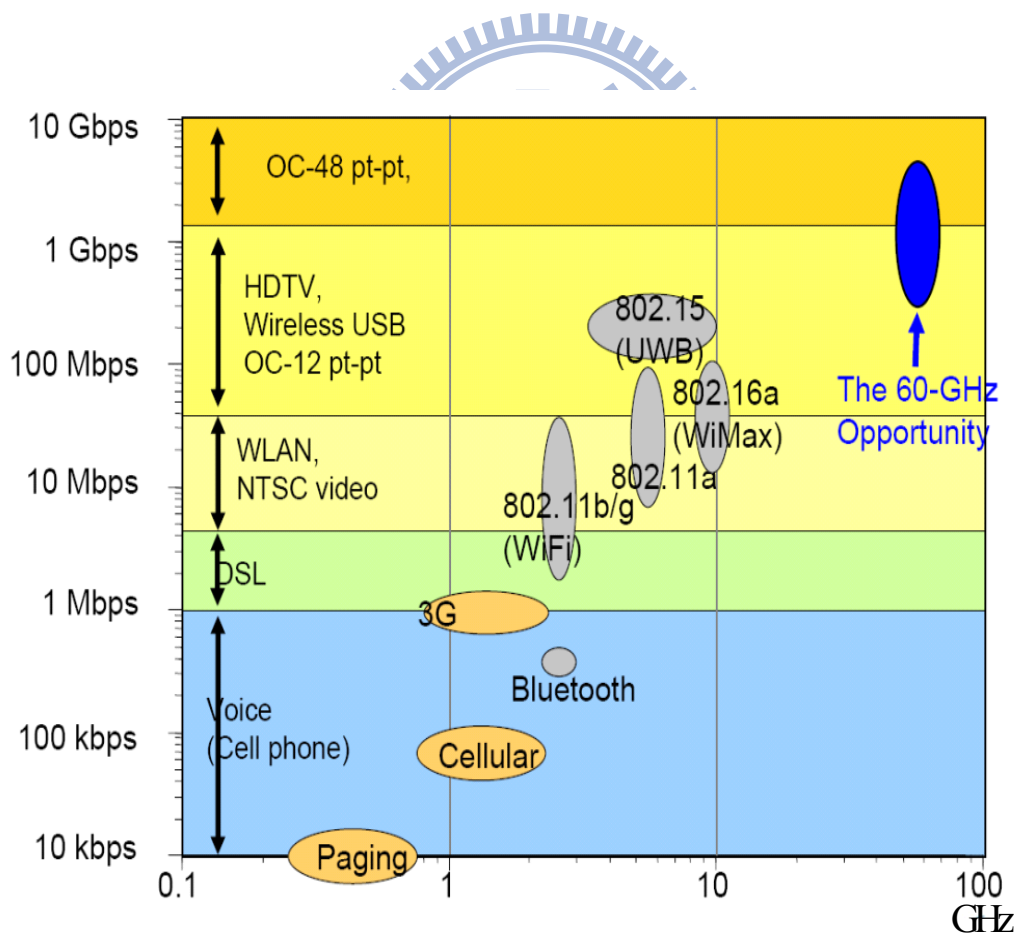
Figure 1-4 Opportunity of 60-GHz RoF system

Chapter 2

Single Sideband Signal by Hilbert Transform

2.1 Introduce of Hilbert Transform

The Hilbert transform H[g(t)] of a signal g(t) is defined as

$$H[g(t)]=g(t)*\frac{1}{\pi t}=\frac{1}{\pi}\int_{-\infty}^{\infty}\frac{\boldsymbol{g}(\tau)}{t-\tau t}\mathrm{d}t=\frac{1}{\pi}\int_{-\infty}^{\infty}\frac{\boldsymbol{g}(\text{t-}\tau)}{\tau t}\mathrm{d}\boldsymbol{t}$$

The Hilbert transform of g(t) is the convolution of g(t) with the signal 1/πt. It is

the response to g(t) of a linear time-invariant filter (called a Hilbert transformer)

having impulse response 1/πt. The Hilbert transform H[g(t)] is often denoted as

g^(t) or as [g(t)]^

A technicality arises immediately. The alert reader will already be concerned

with the definition (1) as the integral is improper: the integrand has a

singularity and the limits of integration are infinite. In fact, the Hilbert

transform is properly defined as the Cauchy principal value of the integral in

(1), whenever this value exists. The Cauchy principal value is defined—for the

first integral in (1)—as

$$H[g(t)]=\frac{1}{\pi}\,l\lim_{\varepsilon\to0^+}\left(\int_{t-1/\varepsilon}^{t-\varepsilon}\frac{\boldsymbol{g}(\tau)}{t-\tau t}\mathrm{d}\boldsymbol{t}+\int_{t+\varepsilon}^{t+1/\varepsilon}\frac{\boldsymbol{g}(\tau)}{t-\tau t}\mathrm{d}\boldsymbol{t}\right)$$

We see that the Cauchy principal value is obtained by considering a finite range

of integration that is symmetric about the point of singularity, but which

excludes a symmetric subinterval, taking the limit of the integral as the length

of the interval approaches ∞ while, simultaneously, the length of the excluded

interval approaches zero. Henceforth, whenever we write an integral as in (1),

we will mean the Cauchy principal value of that integral (when it exists).

Fourier

The signal $1/(\pi t)$ has Fourier transform

$$-j\,\text{sgn}(f)\begin{cases} j-j, & \text{if } f > 0 \\ 0, & \text{if } f = 0 \\ j, & \text{if } f < 0 \end{cases}$$

If g(t) has Fourier transform G(f), then, from the convolution property of the Fourier transform, it follows that g (t) has Fourier transform

$$\hat{G}(f)=-j\,\text{sgn}(f)G(f)$$

Thus, the Hilbert transform is easier to understand in the frequency domain than in the time domain: the Hilbert transform does not change the magnitude of G(f), it changes only the phase. Fourier transform values at positive frequencies are multiplied by $-j$ (corresponding to a phase change of $-\pi/2$) while Fourier transform values at negative frequencies are multiplied by j (corresponding to a phase change of $\pi/2$). Stated yet another way, suppose that G(f) = a + b j for some f . Then G(f) = b − a j if f > 0 and G(f) = −b + a j if f < 0. Thus the Hilbert transform essentially acts to exchange the real and imaginary parts of G(f) (while changing the sign of one of them).

Single-sideband Modulation

For any signal g(t), let

$$g_+(t) = \frac{1}{2}\left[g(t)+j\hat{g}(t)\right]$$

$$g_-(t) = \frac{1}{2}\left[g(t)-j\hat{g}(t)\right]$$

be two complex-valued signals associated with g(t). The significance of these two signals can be seen from their Fourier transforms. We have

$$G_+(f) = \frac{1}{2}[G(f) + j\,\hat{G}(f)] = \frac{1}{2}[G(f)\text{-}j^2\text{sgn}(f)G(f)] = G(f)\frac{1}{2}[1 + \text{sgn}(f)] = G(f)\,u\,(f)$$

where u(f) is the unit step function, and, similarly,

$$G_-(f) = G(f)\,u\,(\text{-}f)$$

Thus g_+(t) has spectral components (equal to those of g(t)) at positive frequencies only, i.e., g_+(t) has a right-sided spectrum. Similarly, g_-(t) has spectral components (equal to those of g(t)) at negative frequencies only and hence has a left-sided spectrum. These spectra are illustrated in Fig. 2-1.
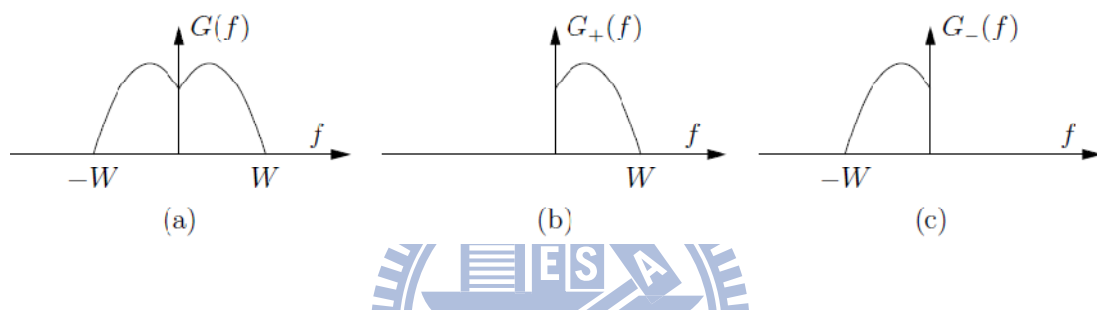
Figure. 2-1 Signal spectra: (a) G(f) (b) the right-sided spectrum G_+(f) (c) the left-sided spectrum G_-(f).

It is now straightforward to express upper- and lower-sideband signals in terms of g_+(t) and g_-(t). Let g(t) be the modulating signal, assumed bandlimited to W Hz, and let f_c > W be the carrier frequency. In the frequency domain, the upper sideband signal is given by

$$S_{USB}(f) = G_+(f\text{-}f_c) + G_-(f+f_c),$$

and the lower sideband signal is given by

$$S_{LSB}(f) = G_-(f\text{-}f_c) + G_+(f+f_c),$$

as sketched in Fig. 2-2 below.
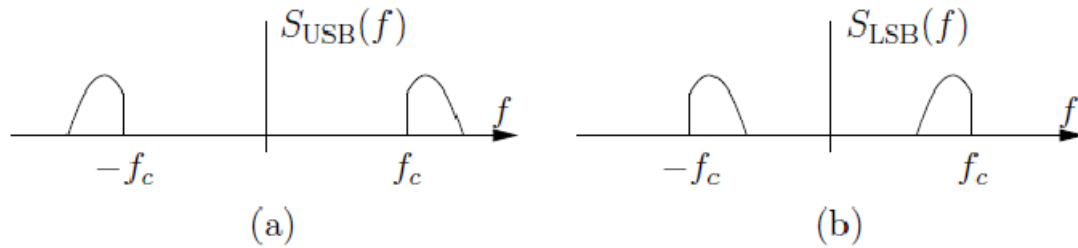
Figure. 2-2 Single-sideband spectra: (a) upper-sideband, (b) lower-sideband

It follows from the frequency-shifting property of the Fourier transform that

$$S_{USB}(f) = g_+(t) \exp(j\,2f_c t) + g_-(t) \exp(-j\,2f_c t)$$

$$= \frac{1}{2}(g(t) + j\,\hat{g}(t)) \exp(j\,2f_c t) + \frac{1}{2}(g(t) - j\,\hat{g}(t)) \exp(-j\,2f_c t)$$

$$= g(t)\frac{1}{2}[\exp(j\,2f_c t) + \exp(-j\,2f_c t)] + \hat{g}(t)\frac{1}{2}[j\exp(j\,2f_c t) - j\exp(-j\,2f_c t)]$$

$$= g(t) \cos(2f_c t) - \hat{g}(t) \sin(2f_c t)$$

A similar derivation shows that

$$S_{LSB}(f) = g(t) \cos(2f_c t) + \hat{g}(t) \sin(2f_c t)$$

Thus we see that single-sideband modulation can be regarded and implemented as a form of quadrature amplitude modulation (QAM), with the modulating signal g(t) placed in the in-phase channel and the Hilbert transform of g(t) (or its negative) placed in the quadrature channel. A block diagram illustrating this approach is given in Fig. 2-3.
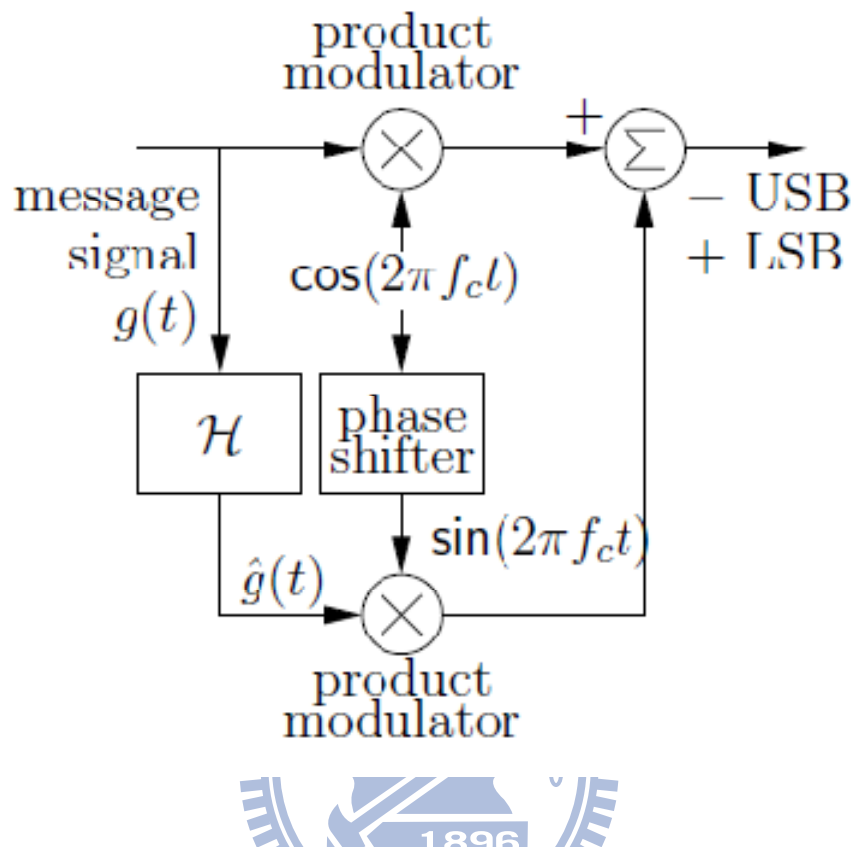
Figure. 2-3 Generation of an SSB-modulated signal

Reference：

F. R. Kschischang, *The Hilbert Transform*,

Department of Electrical and Computer Engineering, University of Toronto,

http://www.comm.toronto.edu/frank/papers/hilbert.pdf

2.2 The Structure of Single Sideband Signal

Figure 2-4 shows the concept of spectra processing of the proposed SSB-QPSK. This modulator consists of two SSB modulators. The configuration of the SSB modulator is shown in Fig. 2-5. Figure 2-4(a) shows the spectra of the I-axis and the Q-axis in conventional QPSK modulation. To realize two times higher throughput, QPSK needs a two times wider bandwidth. (Fig. 2-4(b))

A single side band of the two times wider QPSK is same as the full bandwidth of QPSK. (Fig. 2-4(c)) One of the two SSB signals is turned over on the frequency axis and shifted by a half bandwidth for superimposition. (Fig. 2-4(d))
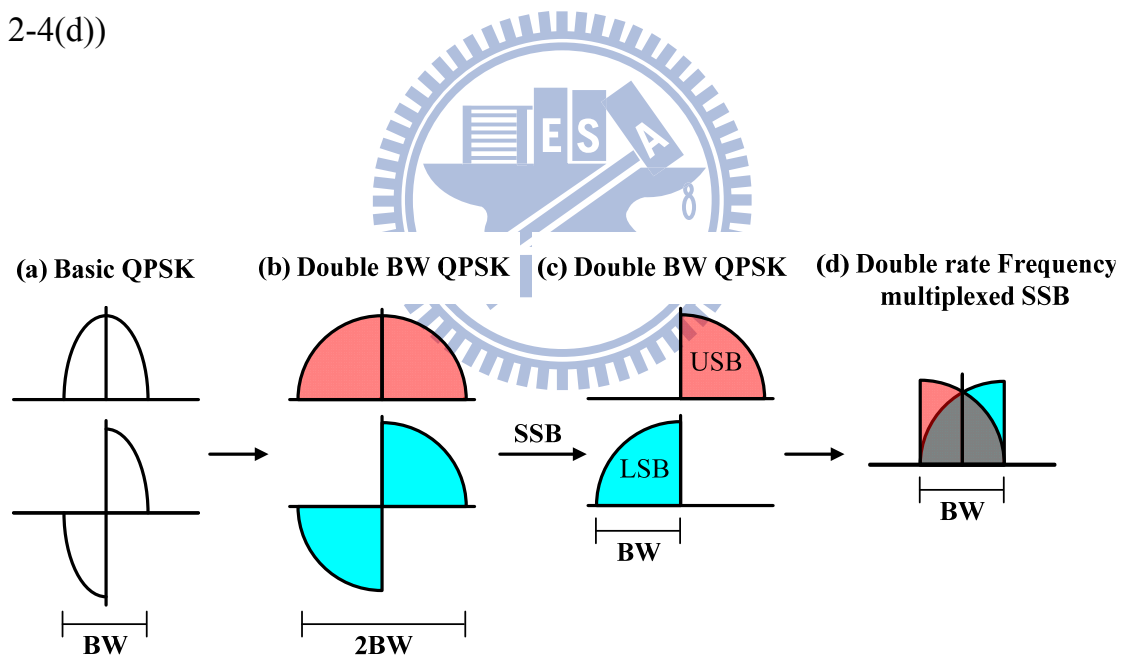
Figure. 2-4 Multiplication of LSB and USB
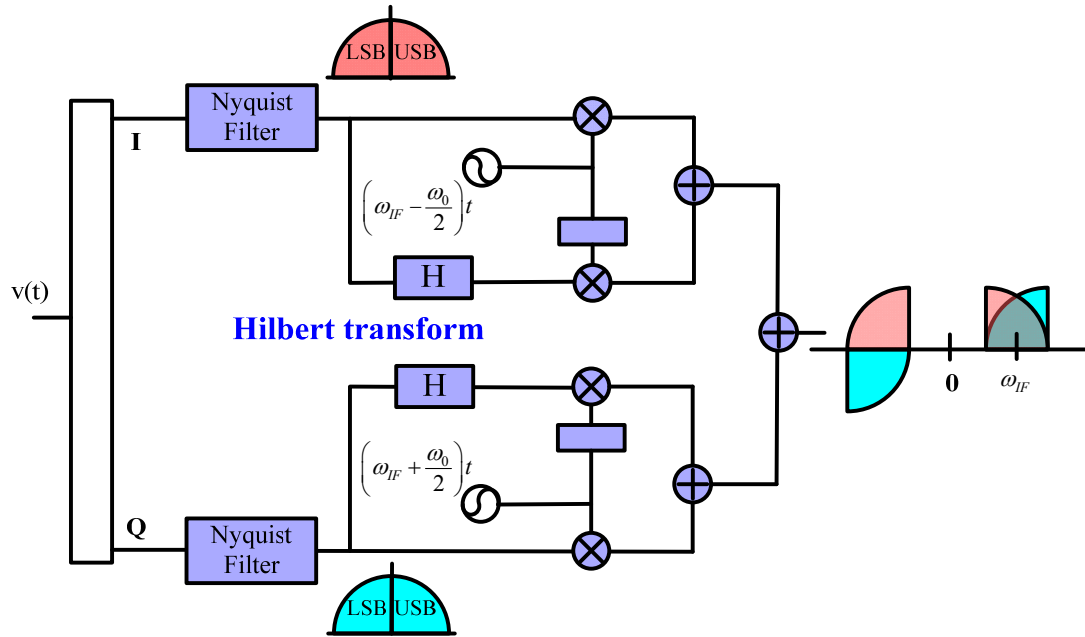
Figure. 2-5 A block diagram of the proposed orthogonal SSB-QPSK

The operation principle of the proposed orthogonal SSB-QPSK method is described using Fig. 2-5. The transmitting signal v(t) passes through a serial to parallel converter and produces two output signals. The upper branch is a multiplier of the input signal and the carrier $\cos\omega 1t$. The lower branch is a multiplier of Hilbert transformed input signal and the $\pi/2$ shifted carrier $\sin\omega 1t$. The throughput can be twice the conventional QPSK, and the paralleled two signal sequences will be referred to as I_k and Q_k, respectively. These two signals pass through Nyquist filters and produce Nyquist wave formed signals. The signal I_k is modulated as the LSB output and is multiplied with $\omega_1 - \omega_0/2$, which is a subtraction of the radio carrier frequency $\omega 1$ and a half of the baseband symbol frequency ω_0. At the same time, the signal Qk is modulated as the USB output and is multiplied with $\omega 1 + \omega_0/2$, which is an addition of $\omega 1$ and a half of the baseband symbol frequency ω_0, where $\omega_0 = \pi T$ is the angular

frequency, and T is the symbol period.

2.3　Matlab Simulation of Single Sideband Signal

Data Format	QPSK
Clock	2.5G
Symbol Rate	2G
Data Rate	4G
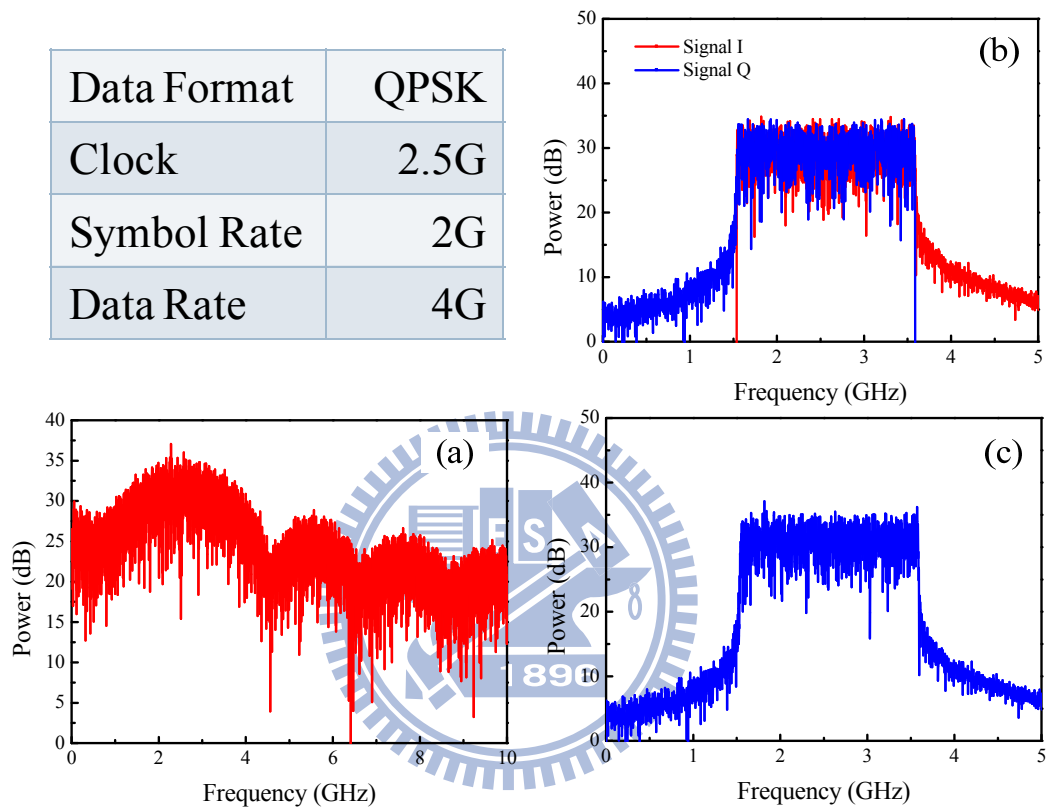
Figure 2-6 Electrical spectrum of (a) Traditional double sideband signal (b) Single sideband signal of I and Q (c) combination of I and Q single sideband signals

According to the block diagrams in Fig. 2-5 a simulation was done. The conditions of simulation are as follows. Figures 2-6 (a), (b) and (c) show the simulation results of the spectrum characteristics orthogonal SSB-QPSK. This simulation results approve that the modulation is an SSB type and has

orthogonal spectrum allocation.

Fig. 2-6 (a) shows the traditional Double Sideband QPSK signal spectrum.
After Hilbert transform process, we can produce a single sideband signal for I
and Q signals (Fig. 2-6 (b)). Fig. 2-6 (c) is the combination of single sideband I,
Q signals.
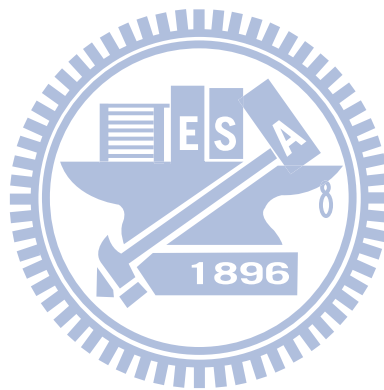
Chapter 3

Introduction of Equalizer

3.1 What Is Inter-symbol Interference

One of the practical problems in digital communications is inter-symbol interference (ISI), which causes a given transmitted symbol to be distorted by other transmitted symbols. ISI occurs because of the channel which has an amplitude and phase dispersion. This dispersion causes the signal to interfere with another parts of the signal. This effect causes to ISI. The ISI is imposed on the transmitted signal due to the band limiting effect of the practical channel, un-even channel frequency response and also due to the multi-path effects of the channel.
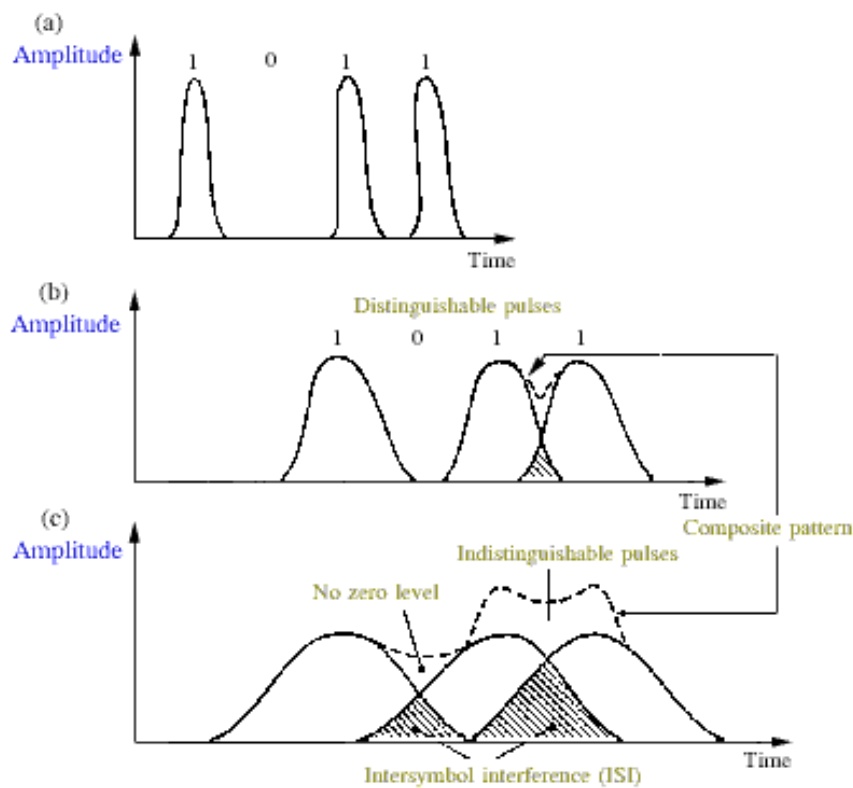
Figure 3-1 Concept of ISI

3.2 Introduction of Equalizer

One of the most commonly used techniques to counter the channel distortion (ISI) is channel equalization. The equalizer is a filter that provides an approximate inverse of the channel response. Since it is common for the channel characteristics to be unknown or to change over time, the preferred embodiment of the equalizer is a structure that is adaptive in nature. Conventional equalization techniques employ a pre-assigned time slot (periodic for the time-varying situation) during which a training signal, known in advance by the receiver, is transmitted. In the receiver the equalizer coefficients are then changed or adapted by using some adaptive algorithm (e.g. LMS, RLS, etc.) so that the output of the equalizer closely matches the training sequence. However, inclusion of this training sequence with the transmitted information adds an overhead and thus reduces the throughput of the system. Therefore, to reduce the system overhead, adaptation schemes are preferred that do not require training, i.e., blind adaptation schemes. In blind equalization, instead of using the training sequence, one or more properties of the transmitted signal are used to estimate the inverse of the channel. Figure 3-2 depicts the response to a single transmit pulse at various points in the system.
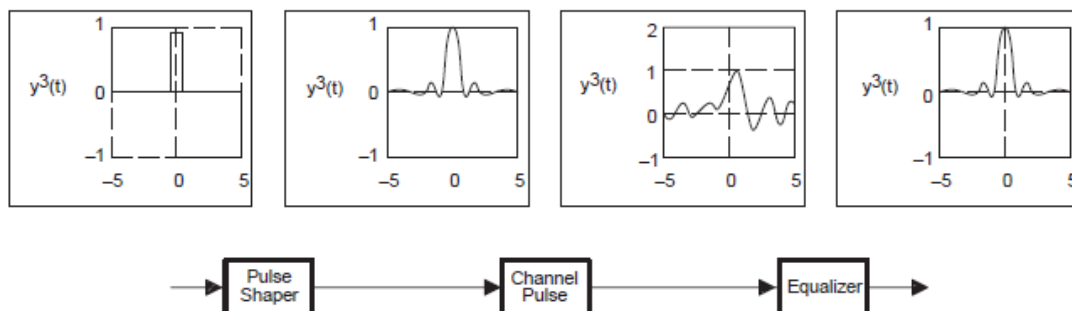
Figure 3-2 Transmission process with example pulse responses

3.3 Concept of Feed-forward Equalizer and Decision Feedback Equalizer

Symbol-Spaced Equalizers (Feed-forward Equalizer)

A symbol-spaced linear equalizer consists of a tapped delay line that stores samples from the input signal. Once per symbol period, the equalizer outputs a weighted sum of the values in the delay line and updates the weights to prepare for the next symbol period. This class of equalizer is called symbol-spaced because the sample rates of the input and output are equal. Below is a schematic of a symbol-spaced linear equalizer
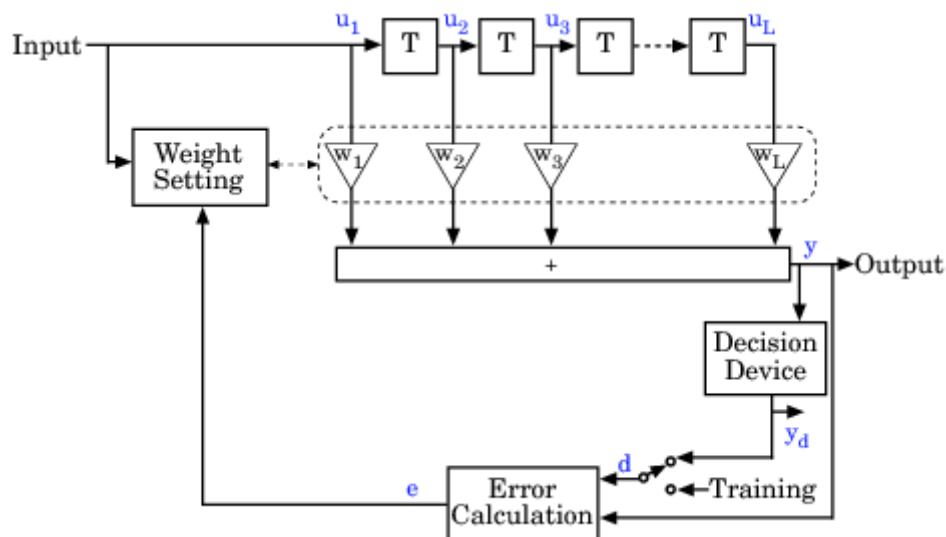
Figure 3-3 Schematic of a symbol-spaced linear equalizer

Decision-Feedback Equalizers

A decision-feedback equalizer is a nonlinear equalizer that contains a forward filter and a feedback filter. The forward filter is similar to the linear equalizer described in Symbol-Spaced Equalizers, while the feedback filter contains a tapped delay line whose inputs are the decisions made on the

equalized signal. The purpose of a DFE is to cancel inter-symbol interference while minimizing noise enhancement. By contrast, noise enhancement is a typical problem with the linear equalizers described earlier.

Below is a schematic of a fractionally spaced DFE with L forward weights and N-L feedback weights. The forward filter is at the top and the feedback filter is at the bottom. If K is 1, the result is a symbol-spaced DFE instead of a fractionally spaced DFE.
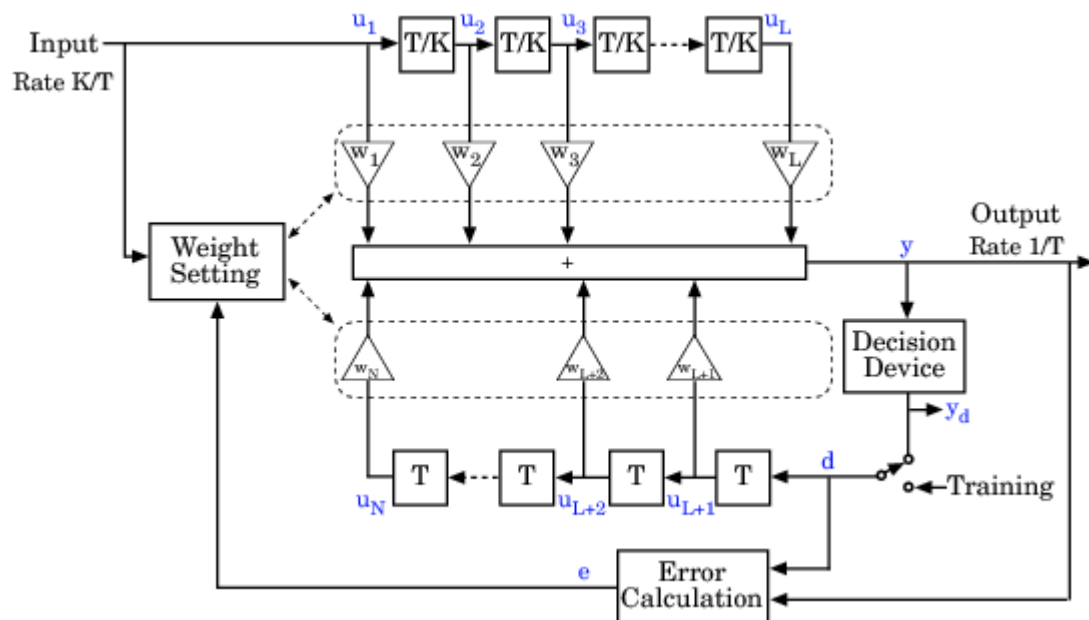
Figure 3-4 Schematic of a decision feedback equalizer

In each symbol period, the equalizer receives K input samples at the forward filter, as well as one decision or training sample at the feedback filter. The equalizer then outputs a weighted sum of the values in the forward and feedback delay lines, and updates the weights to prepare for the next symbol period.

3.4 Algorithm
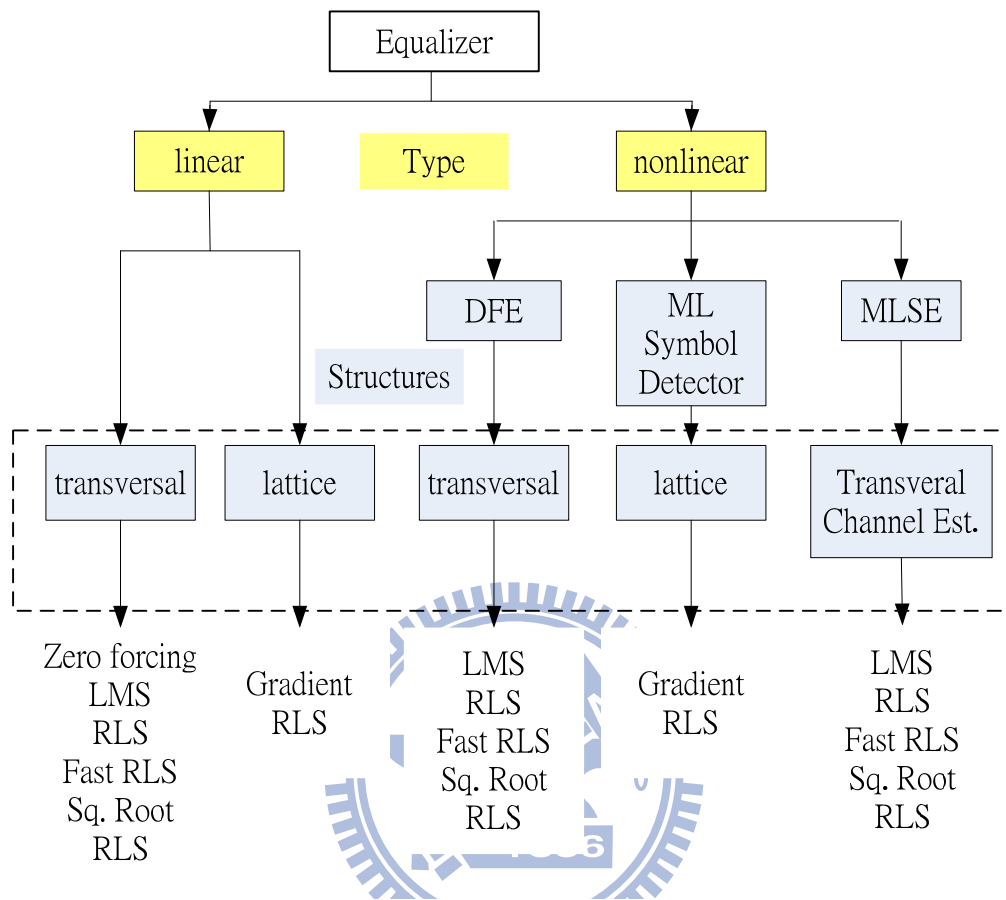
Figure 3-5 Sorts of equalizers

In the design of equalizers there exist different types of design criteria [25]. The most frequently encountered two criteria with their efficiency are told in the sequel. Some equalizers are designed to minimize mean square error (MSE) at the slicer input with the constraint of zero ISI. These are called Zero-Forcing (ZF) equalizers. Some equalizers are designed to minimize the MSE at the input of the slicer by reducing the signal slightly at the slicer input. This reduction of signal results in reduction in MSE, so overall MSE is smaller than that of the ZF equalizer. These equalizers are called MSE equalizers. The MSE equalizer is generally preferred against ZF equalizer because of less noise

enhancement.

The linear equalizer is cheap in implementation but its noise performance is not very good. So, in the literatures, some equalizer types which introduce nonlinearity are searched. The most popular of these nonlinear equalizers is the decision feedback equalizer (DFE). The DFE is first proposed by Austin in [27]. This equalizer results in less MSE against linear equalizer, but it has the disadvantage of error propagation in its feedback loop.

As it is told before, most of the time, the channel's and, consequently, the transmission system's transfer functions are not known. Also, the channel's impulse response may vary with time and fade. The result of this is that the equalizer can't be designed a priori, frequently. So, mostly preferred scheme is to exploit adaptive equalizers. Adaptive equalizers use adaptive algorithms to converge to the true coefficients and have the benefit of tracking the changes in the channel impulse response. But, to achieve this, it adds additional complexity to the receiver structure.

Also, the adaptation algorithm plays a significant role for the performance of the equalizer. The most popular algorithm from the aspect of performance and complexity is the Least Mean Squares (LMS) algorithm. It has a good performance and low complexity. It is globally convergent if the desired values are given correctly. The handicap of LMS algorithm for equalizer if the desired symbols are not correct, it does not converge. So, the equalizer using LMS algorithm requires a priori known symbols in case the decisions of the equalizer are wrong.

The LMS algorithm is a linear adaptive filtering algorithm that belongs to the family of the stochastic gradient algorithms [26]. The stochastic gradient

algorithms differ from the steepest descent algorithms in that the gradient is not calculated deterministically. The LMS algorithm has two parts. In the first part, the output of a transversal filter is computed according to the tap inputs and the error term is generated according to the difference between the filter output and the desired response. In the second part, the adjustment of the tap weights is done according to the error term.

The algorithm forms a feedback loop by the error term fed back. The filter produces an output and the difference between the output and the desired term is obtained. This difference is the estimation error term. The estimation error is given to the Adaptation Control Block. Adaptation Control Block multiplies the estimation error with the input taps' complex conjugate and a step size α. The results of the corresponding taps are added to the corresponding filter taps. So, the new filter is obtained [24]:

$$e(k)=I(k)-Q(k)=I(k)-f^T(k)\cdot\hat{r}(k) \tag{2.1}$$

$$f(k+1)=f(k)+\alpha\cdot\hat{r}^*(k)\cdot e(k) \tag{2.2}$$

$$f_n(k+1)=f_n(k)+\alpha\cdot\hat{r}^*(k-n)\cdot e(k) \quad 0\le n\le M\text{-}1 \tag{2.3}$$

where f(k) is the filter vector at time k, and rˆ* (k) is the complex conjugate of the input vector at time k, α is the step size parameter, e(k) is the estimation error, I(k) is the desired response at time k. In equation (2.3), fn(k) is the nth tap of the filter at time k, and r*(k-n) is the complex conjugate of the input at time k-n, and other parameters are the same as first equation. Equations (2.2) and (2.3) are equivalent. The small step size will result in less excess error but in slow convergence rate. The large step size will result in high excess error but high convergence rate.

Chapter 4

The Concept of New Optical Modulation System

4.1 Preface

There are three parts in optical communication systems : optical transmitter, communication channel and optical receiver. Optical transmitter converts an electrical input signal into the corresponding optical signal and then launches it into the optical fiber serving as a communication channel. The role of an optical receiver is to convert the optical signal back into electrical form and recover the data transmitted through the lightwave system. In this chapter, we will do an introduction about the external Mach-Zehnder Modulator (MZM), constructing a model of new ROF system.

4.2 Mach-Zehnder Modulator (MZM)

Direct modulation and external modulation are two modulations of generated optical signal. When the bit rate of direct modulation signal is above 10 Gb/s, the frequency chirp imposed on signal becomes large enough. Hence, it is difficult to apply direct modulation to generate microwave/mm-wave. However, the bandwidth of signal generated by external modulator can exceed 10 Gb/s. Presently, most RoF systems are using external modulation with Mach-Zehnder modulator (MZM) or Electro-Absorption Modulator (EAM). The most commonly used MZM are based on LiNbO3 (lithium niobate) technology. According to the applied electric field, there are two types of LiNbO3 device : x-cut and z-cut.   According to number of electrode, there are two types of LiNbO3 device: dual-drive Mach-Zehnder modulator (DD-MZM)

and single-drive Mach-Zehnder modulator (SD-MZM) [6].

4.3 Single-drive Mach-Zehnder modulator

The SD-MZM has two arms and an electrode. The optical phase in each arm can be controlled by changing the voltage applied on the electrode. When the lightwaves are in phase, the modulator is in "on" state. On the other hand, when the lightwaves are in opposite phase, the modulator is in "off" state, and the lightwave cannot propagate by waveguide for output.

4.4 The architecture of ROF system

4.4.1 Optical transmitter

Optical transmitter concludes optical source, optical modulator, RF signal, electrical mixer, electrical amplifier, etc.. Presently, most RoF systems are using laser as light source. The advantages of laser are compact size, high efficiency, good reliability small emissive area compatible with fiber core dimensions, and possibility of direct modulation at relatively high frequency. The modulator is used for converting electrical signal into optical form. Because the external integrated modulator was composed of MZMs, we select MZM as modulator to build the architecture of optical transmitter.

There are two schemes of optical transmitter generated optical signal. One scheme is used two MZM. First MZM generates optical carrier which carried the data. The output optical signal is BB signal. The other MZM generates optical subcarrier which carried the BB signal and then output the RF signal, as shown in Fig. 4-1 (a). The other scheme is used a mixer to get up-converted electrical signal and then send it into a MZM to generate the optical signal, as

shown in Fig. 4-1 (b). Fig. 4-1 (c) shows the duty cycle of subcarrier biased at different points in the transfer function.
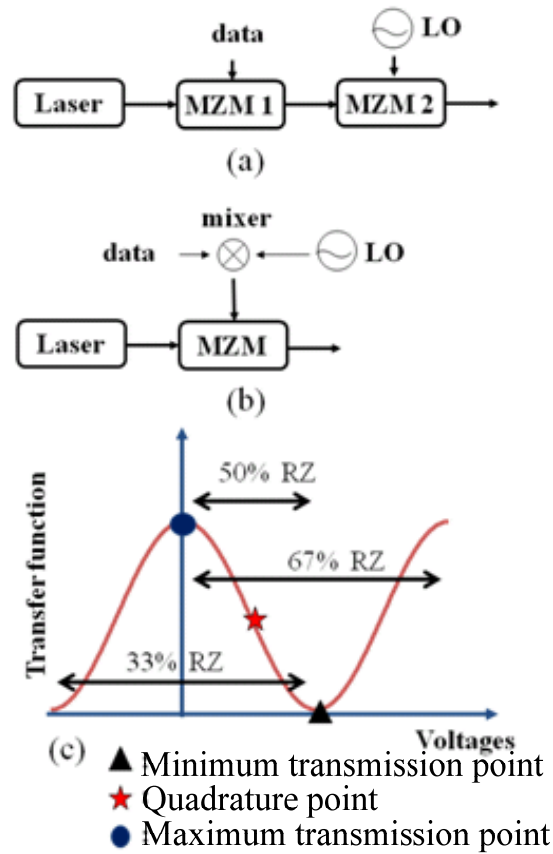
Figure 4-1 (a) and (b) are two schemes of transmitter and (c) is duty cycle of subcarrier biased at different points in the transfer function. (LO: local oscillator)

4.4.2　Optical signal generations based on LiNbO3 MZM
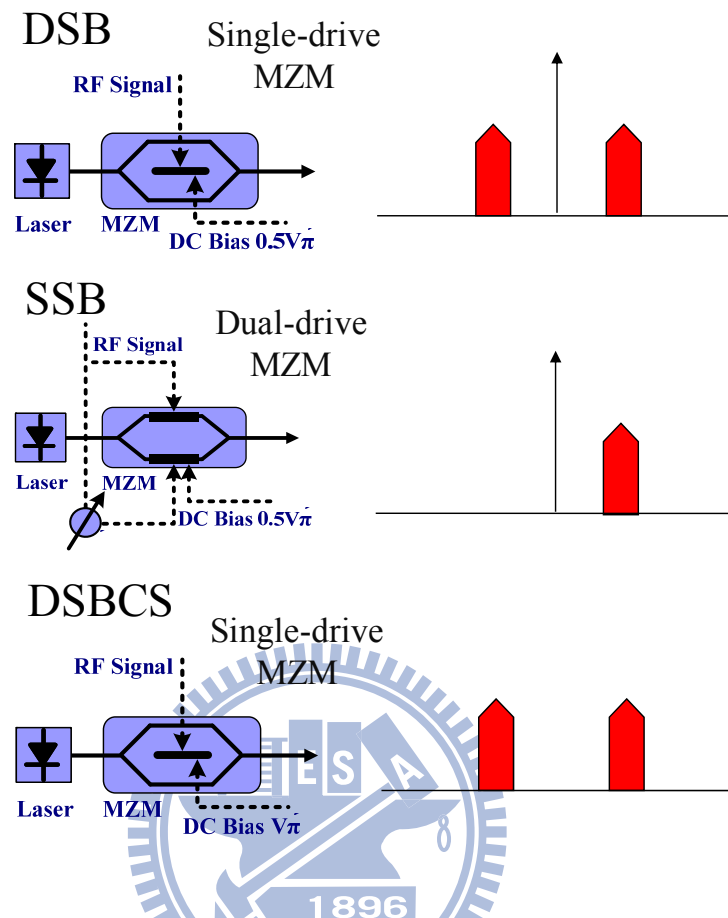
Figure 4-2 Optical microwave/mm-wave modulation scheme by using MZM.

The microwave and mm-wave generations are key techniques in RoF systems. The optical mm-waves using external MZM based on double-sideband (DSB), single-sideband (SSB), and double-sideband with optical carrier suppression (DSBCS) modulation schemes have been demonstrated, as shown in Fig. 4-2. Generated optical signal by setting the bias voltage of MZM at quadrature point, the DSB modulation experiences performance fading problems due to fiber dispersion, resulting in degradation of the receiver sensitivity. When an optical signal is modulated by an electrical RF signal, fiber chromatic dispersion causes the detected RF signal power to

have a periodic fading characteristic. The DSB signals can be transmitted over several kilo-meters. Therefore, the SSB modulation scheme is proposed to overcome fiber dispersion effect. The SSB signal is generated when a phase difference of π/2 is applied between the two RF electrodes of the DD-MZM biased at quadrature point. Although the SSB modulation can reduce the impairment of fiber dispersion, it suffers worse receiver sensitivity due to limited optical modulation index (OMI). The DSBCS modulation is demonstrated optical mm-wave generation using DSBCS modulation. It has no performance fading problem and it also provides the best receiver sensitivity because the OMI is always equal to one. The other advantage is that the bandwidth requirement of the transmitter components is less than DSB and SSB modulation. However, the drawback of the DSBCS modulation is that it can't support vector signals, such as phase shift keying (PSK), quadrature amplitude modulation (QAM), or OFDM signals, which are of utmost importance in wireless applications.

4.4.3 Communication channel

Communication channel concludes fiber, optical amplifier, etc.. Presently, most RoF systems are using single-mode fiber (SMF) or dispersion compensated fiber (DCF) as the transmission medium. When the optical signal transmits in optical fiber, dispersion will be happened. DCF is use to compensate dispersion. The transmission distance of any fiber-optic communication system is eventually limited by fiber losses. For long-haul systems, the loss limitation has traditionally been overcome using regenerator witch the optical signal is first converted into an electric current and then

regenerated using a transmitter. Such regenerators become quite complex and expensive for WDM lightwave systems. An alternative approach to loss management makes use of optical amplifiers, which amplify the optical signal directly without requiring its conversion to the electric domain [28]. Presently, most RoF systems are using erbium-doped fiber amplifier (EDFA). An optical band-pass filter (OBPF) is necessary to filter out the ASE noise. The model of communication channel is shown in Fig. 4-3.
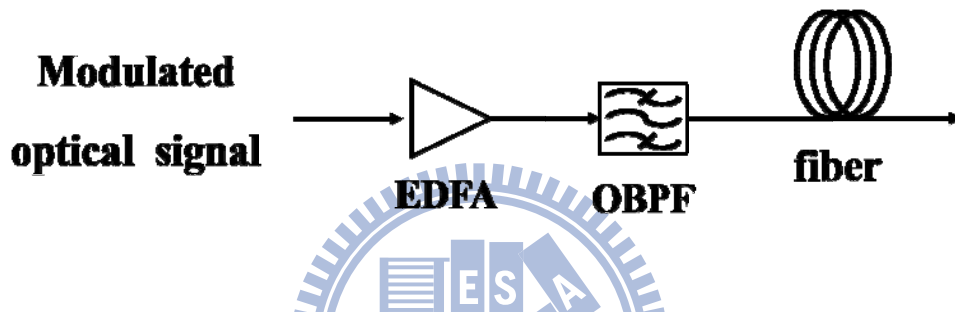
Figure 4-2 The model of communication channel in a RoF system.

4.4.4 Demodulation of optical millimeter-wave signal

Optical receiver concludes photo-detector (PD), demodulator, etc.. PD usually consists of the photo diode and the trans-impedance amplifier (TIA). In the microwave or the mm-wave system, the PIN diode is usually used because it has lower transit time. The function of TIA is to convert photo-current to output voltage.

The BB and RF signals are identical after square-law photo detection. We can get RF signal by using a mixer to drop down RF signal to baseband then filtered by low-pass filter (LPF).

After getting down-converted signal, it will be sent into a signal tester to test the quality, just like bit-error-rate (BER) tester or oscilloscope, as shown in

Fig. 4-4.

Combining the transmitter with communication channel and receiver, that is the model of ROF system, as shown in Fig. 4-5. We select the scheme of Fig. 4-3 (b) to become the transmitter in the model of ROF system.

Figure 4-3 The model of receiver in a ROF system.
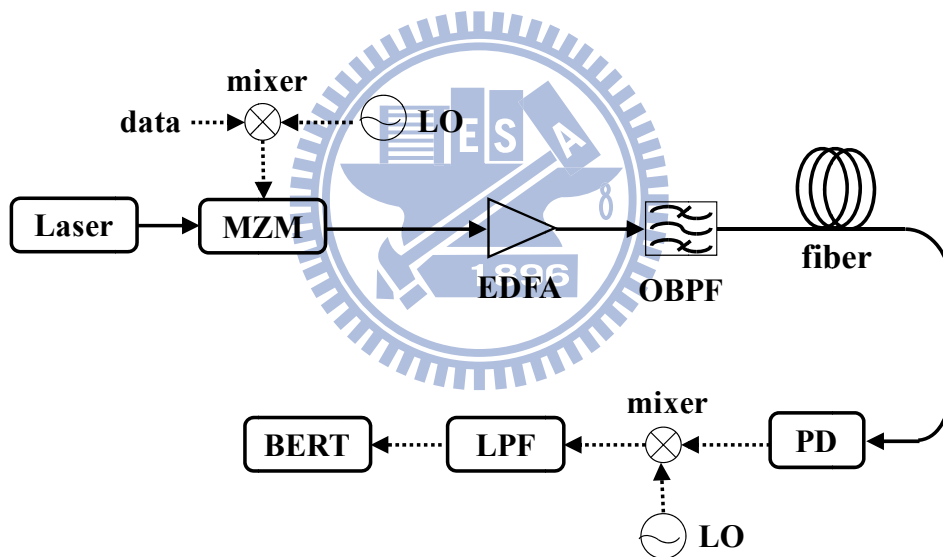
Figure 4-4 The model of ROF system.

4.5 The new proposed model of optical modulation system
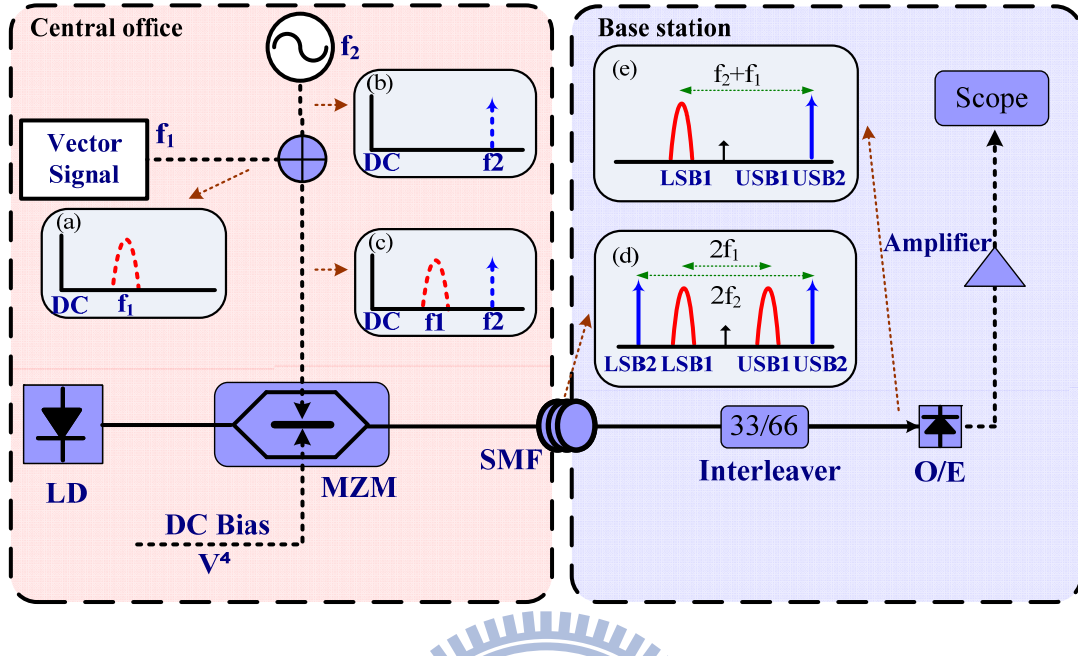
Figure 4-6 The proposed RoF system based on a single-electrode MZM.

Figure 4-6 schematically depicts the concept of the proposed RoF system. The MZM driving signal at a subcarrier frequency of f_1 and a sinusoidal LO signal with a frequency of f_2, as indicated in insets (a)-(c) of Fig. 4-6 The frequency, f_2 of the LO signal is half the desired mm-wave frequency of operation. To achieve the double sideband with carrier suppression (DSBCS) modulation scheme, the MZM is biased at the null point to suppress the optical carrier. Inset (d) of Fig. 4-6 shows the generated optical signal and LO spectrum that has two upper-wavelength sidebands (USB1, USB2) and two lower-wavelength sidebands (LSB1, LSB2) with carrier suppression at the output of the MZM. After square-law photo detection, the generated photocurrent can be written as

$$I_{photo} = (USB1+USB2+LSB1+LSB2)^2.$$

(1)

Expanding the above equation produces the following terms:

$$DC = USB1^2 + USB2^2 + LSB1^2 + LSB2^2. \tag{2}$$

Signal at the sum frequency=

$$USB1 \times LSB2 + USB2 \times LSB1. \tag{3}$$

Signal at the frequency difference=

$$USB1 \times USB2 + LSB1 \times LSB2. \tag{4}$$

$$\text{Beat noise} = USB1 \times LSB1 + USB2 \times LSB2. \tag{5}$$

The beating terms of USB1 × LSB2 and USB2 × LSB1 generate the desired electrical signals at the sum frequency (f2+f1). The beating terms of USB1 × USB2 and LSB1 × LSB2 generate electrical signals at the frequency difference (f2-f1), which are well below the desired mm-wave frequency band and are filtered off by low-pass filter at receiver part. Notably, a frequency multiplication factor of two (2) can be achieved by properly choosing frequencies f1 and f2. This reduces the bandwidth requirements of the RoF transmitter allowing for the use of low-frequency electrical and optical components, including the MZM (< 40 GHz), which are readily available and have very good performance (e.g. flat frequency response).

In this system, the target sum frequency is 60 GHz. Two main issues will be crucial to the system performance and will be explained in details in following. First, the RF fading issue, as shown in the equation (12), comes from the interaction between the two copies of the desired signals, which are generated at the photodiode, namely USB1 × LSB2 and USB2 × LSB1, respectively. After fiber transmission, the relative phase between the two generated RF signals will change with transmitted distance owing to the slight difference in the propagation speeds of the two sideband pairs induced by fiber chromatic dispersion. As the relative phase reaches 180°, the electrical RF signal will

vanish. This is the RF fading problem. Here is also the reason why we use an interleaver to filter out USB1 and LSB2. The second issue comes from beat noise of two signals USB1 × LSB1. If the center frequency of single carrier signals is not properly chosen, the beat noise will fall into the signal band and severely degrade the system performance.
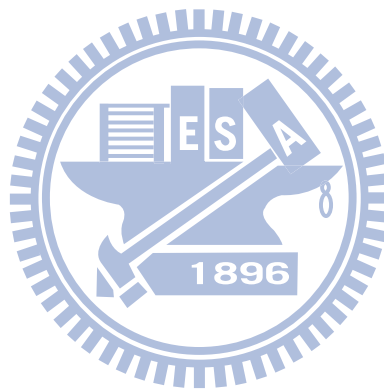
Chapter 5

The Theoretical Calculations of Proposed System

5.1   Introduce MZM

For MZM with configuration as Fig. 5-1, the output E-filed for upper arm is

$$E_U = E_0 \cdot a \cdot e^{j\Delta\varphi_1} \tag{1}$$

$$\Delta\varphi_1 \triangleq \frac{v_1}{v_\pi} \cdot \pi \tag{2}$$

$\Delta\varphi_1$ is the optical carrier phase difference that is induced by v_1, where a is the power splitting ratio.

The output E-filed for upper arm is

$$E_L = E_0 \cdot \sqrt{1 - a^2} \cdot e^{j\Delta\varphi_2} \tag{3}$$

$\Delta\varphi_2$ is the optical carrier phase difference that is induced by v_2

$$\Delta\varphi_2 \triangleq \frac{v_2}{v_\pi} \cdot \pi \tag{4}$$

The output E-filed for MZM is

$$E_T = E_0 \cdot \left\{ a \cdot b \cdot e^{j\Delta\varphi_1} + \sqrt{1 - a^2} \cdot \sqrt{1 - b^2} \cdot e^{j\Delta\varphi_2} \right\} \tag{5}$$

where a and b are the power splitting ratios of the first and second Y-splitters in MZM, respectively. The power splitting ratio of two arms of a balanced MZM is 0.5. The electrical field at the output of the MZM is given by

$$E_T = \frac{1}{2} \cdot E_0 \cdot \left\{ e^{j\Delta\varphi_1} + e^{j\Delta\varphi_2} \right\} \tag{6}$$

$$E_T = E_0 \cdot \cos\left(\frac{\Delta\varphi_1 - \Delta\varphi_2}{2} \right) \cdot \exp\left(j\frac{\Delta\varphi_1 + \Delta\varphi_2}{2} \right) \tag{7}$$

For single electro x-cut MZM. The electrical field at the output is given by

$$E_{OUT} = E_0 \cdot \cos\left(\frac{\Delta\varphi - (-\Delta\varphi)}{2} \right) \cdot \exp\left(j\frac{\Delta\varphi + (-\Delta\varphi)}{2} \right) \tag{8}$$

Add time component, the electrical field is

$$E_{OUT} = E_0 \cdot \cos(\Delta\varphi) \cdot \cos(\omega_0 t) \tag{9}$$

where E_0 and ω_c denote the amplitude and angular frequency of the input optical carrier, respectively; $V(t)$ is the applied driving voltage, and $\Delta\varphi$ is the optical carrier phase difference that is induced by $V(t)$ between the two arms of the MZM. The loss of MZM is neglected. $V(t)$ consisting of an electrical sinusoidal signal and a dc biased voltage can be written as,

$$V(t) = V_{bias} + V_m \cos(\omega t) \tag{10}$$

where V_{bias} is the dc biased voltage, V_m and ω_{RF} are the amplitude and the angular frequency of the electrical driving signal, respectively. The optical carrier phase difference induced by $V(t)$ is given by

$$\Delta\varphi = \frac{V(t)}{2V_\pi} = \frac{V_{bias} + V_m \cos(\omega t)}{V_\pi} \cdot \frac{\pi}{2} \tag{11}$$

Eq. (10) can be written as:

$$
\begin{aligned}
E_{OUT} &= E_0 \cdot \cos\left[\frac{V_{bias} + V_m \cos(\omega t)}{V_\pi} \cdot \frac{\pi}{2}\right] \cdot \cos(\omega_0 t) \\
&= E_0 \cdot \cos[b + m \cdot \cos(\omega_{RF} t)] \cdot \cos(\omega_0 t) \\
&= E_0 \cdot \cos(\omega_0 t) \cdot \{\cos(b) \cdot \cos[m \cdot \cos(\omega_{RF} t)] \\
&\qquad\qquad - \sin(b) \cdot \sin[m \cdot \cos(\omega_{RF} t)]\}
\end{aligned} \tag{12}
$$

where $b \triangleq \frac{V_{bias}}{2V_\pi}\pi$ is a constant phase shift that is induced by the dc biased voltage, and $m \triangleq \frac{V_m}{2V_\pi}\pi$ is the phase modulation index.

$$
\begin{cases}
\cos(x \sin\theta) = J_0(x) + 2\displaystyle\sum_{n=1}^{\infty} J_{2n}(x) \cos(2n\theta) \\
\sin(x \sin\theta) = 2\displaystyle\sum_{n=1}^{\infty} J_{2n-1}(x) \sin[(2n-1)\theta]
\end{cases}
$$

$$\begin{cases} \cos(x\cos\theta) = J_0(x) + 2\sum_{n=1}^{\infty}(-1)^n J_{2n}(x)\cos(2n\theta) \\ \sin(x\cos\theta) = 2\sum_{n=1}^{\infty}(-1)^n J_{2n-1}(x)\cos[(2n-1)\theta] \end{cases}$$

$$(13)$$

Expanding Eq. (12) using Bessel functions, as detailed in Eq. (13). The electrical field at the output of the MZM can be written as:

$$E_{OUT} = E_0 \cdot \cos(\omega_0 t) \cdot$$

$$\{\cos(b) \cdot [J_0(m) + 2 \cdot \sum_{i=1}^{\infty}(-1)^n \cdot J_{2n}(m) \cdot \cos(2n\omega_{RF}t)]$$

$$-\sin(b) \cdot [2 \cdot \sum_{i=1}^{\infty}(-1)^n \cdot J_{2n-1}(m) \cdot \cos[(2n-1)\omega_{RF}t]]\}$$

$$(14)$$

where J_n is the Bessel function of the first kind of order n. the electrical field of the mm-wave signal can be written as

$$E_{OUT} = E_0 \cdot \cos(b) \cdot J_0(m) \cdot \cos(\omega_0 t)$$

$$+E_0 \cdot \cos(b) \cdot \sum_{i=1}^{\infty} J_{2n}(m) \cdot \cos[(\omega_0 - 2n\omega_{RF})t + n\pi]$$

$$+E_0 \cdot \cos(b) \cdot \sum_{i=1}^{\infty} J_{2n}(m) \cdot \cos[(\omega_0 + 2n\omega_{RF})t + n\pi]$$

$$-E_0 \cdot \sin(b) \cdot \sum_{i=1}^{\infty} J_{2n-1}(m) \cdot \cos[\omega_0 - (2n-1)\omega_{RF})t + n\pi]$$

$$-E_0 \cdot \sin(b) \cdot \sum_{i=1}^{\infty} J_{2n-1}(m) \cdot \cos[\omega_0 + (2n-1)\omega_{RF})t + n\pi]$$

$$(15)$$
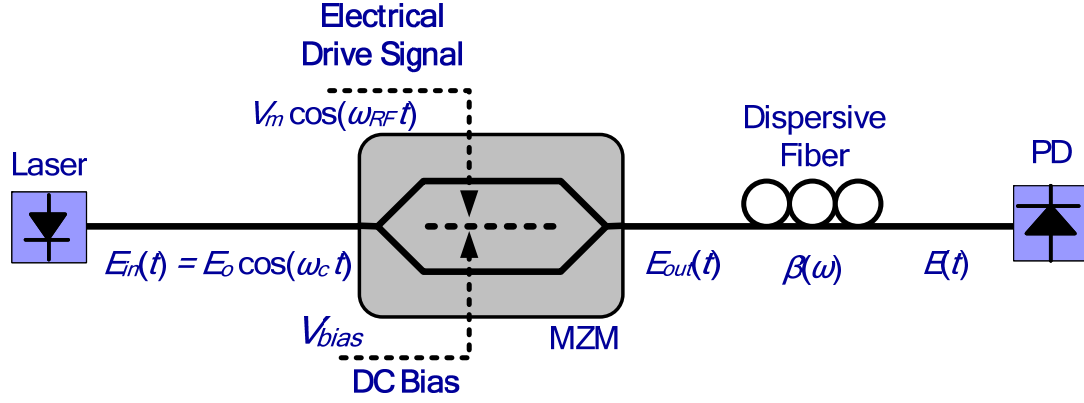
Figure 5-1 The principle diagram of the optical mm-wave generation using balanced MZM.

5.2 Theoretical calculation of single drive MZM

5.2.1 Bias at maximum transmission point

When the MZM is biased at the maximum transmission point, the bias voltage is set at $V_{bias} = 0$, and $\cos b = 1$ and $\sin b = 0$. Consequently, the electrical field of the mm-wave signal can be written as

$$E_{OUT}(t) = E_0 \cdot J_0(m) \cdot \cos(\omega_0 t)$$

$$+ E_0 \cdot \sum_{n=1}^{\infty} J_{2n}(m) \cdot \cos[(\omega_0 - 2n\omega_{RF})t + n\pi]$$

$$+ E_0 \cdot \sum_{n=1}^{\infty} J_{2n}(m) \cdot \cos[(\omega_0 + 2n\omega_{RF})t + n\pi]$$

(16)

The amplitudes of the generated optical sidebands are proportional to those of the corresponding Bessel functions associated with the phase modulation index m. With the amplitude of the electrical driving signal V_m equal to V_π, the maximum m is $\frac{\pi}{2}$. As $0 < m < \frac{\pi}{2}$, the Bessel function J_n for $n \geq 1$

decreases and increases with the order of Bessel function and m, respectively, as shown in Figure 5-2. $J_1\left(\frac{\pi}{2}\right)$, $J_2\left(\frac{\pi}{2}\right)$, $J_3\left(\frac{\pi}{2}\right)$, and $J_4\left(\frac{\pi}{2}\right)$ are 0.5668, 0.2497, 0.069, and 0.014, respectively. Therefore, the optical sidebands with the Bessel function higher than $J_3(m)$ can be ignored, and Eq. (14) can be further simplified to

$$E_{OUT} = E_0 \cdot J_0(m) \cdot \cos(\omega_0 t)$$
$$+E_0 \cdot J_2(m) \cdot \cos\left[(\omega_0 - 2\omega_{RF})t + \pi\right]$$
$$+E_0 \cdot J_2(m) \cdot \cos\left[(\omega_0 + 2\omega_{RF})t + \pi\right]$$
$$+E_0 \cdot J_4(m) \cdot \cos\left[(\omega_0 - 4\omega_{RF})t\right]$$
$$+E_0 \cdot J_4(m) \cdot \cos\left[(\omega_0 + 4\omega_{RF})t\right] \tag{17}$$
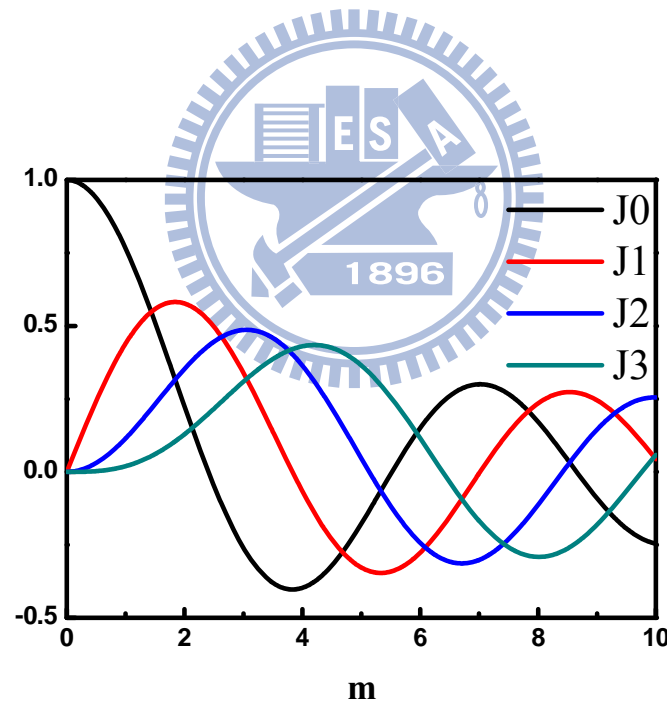
Figure 5-2 The different order of Bessel functions vs. m.

5.2.2 Bias at quadrature point

When the MZM is biased at the quadrature point, the bias voltage is set at

$V_{bias} = \frac{V_\pi}{2}$, and $\cos b = \frac{\sqrt{2}}{2}$ and $\sin b = \frac{\sqrt{2}}{2}$. Consequently, the electrical field of the mm-wave signal can be written as

$$
\begin{aligned}
E_{OUT} = \; & \frac{1}{\sqrt{2}} \cdot E_0 \cdot J_0(m) \cdot \cos(\omega_0 t) \\
& + \frac{1}{\sqrt{2}} \cdot E_0 \cdot J_1(m) \cdot \cos\left[(\omega_0 - \omega_{RF})t\right] \\
& + \frac{1}{\sqrt{2}} \cdot E_0 \cdot J_1(m) \cdot \cos\left[(\omega_0 + \omega_{RF})t\right] \\
& + \frac{1}{\sqrt{2}} \cdot E_0 \cdot J_2(m) \cdot \cos\left[(\omega_0 - 2\omega_{RF})t + \pi\right] \\
& + \frac{1}{\sqrt{2}} \cdot E_0 \cdot J_2(m) \cdot \cos\left[(\omega_0 + 2\omega_{RF})t + \pi\right] \\
& + \frac{1}{\sqrt{2}} \cdot E_0 \cdot J_3(m) \cdot \cos\left[(\omega_0 - 3\omega_{RF})t + \pi\right] \\
& + \frac{1}{\sqrt{2}} \cdot E_0 \cdot J_3(m) \cdot \cos\left[(\omega_0 + 3\omega_{RF})t + \pi\right]
\end{aligned}
$$

(18)

5.2.3 Bias at null point

When the MZM is biased at the null point, the bias voltage is set at $V_{bias} = V_\pi$, and $\cos b = 0$ and $\sin b = 1$. Consequently, the electrical field of the mm-wave signal using DSBCS modulation can be written as

$$
\begin{aligned}
E_{OUT} = \; & E_0 \cdot J_1(m) \cdot \cos\left[(\omega_0 - \omega_{RF})t\right] \\
& + E_0 \cdot J_1(m) \cdot \cos\left[(\omega_0 + \omega_{RF})t\right] \\
& + E_0 \cdot J_3(m) \cdot \cos\left[(\omega_0 - 3\omega_{RF})t + \pi\right] \\
& + E_0 \cdot J_3(m) \cdot \cos\left[(\omega_0 + 3\omega_{RF})t + \pi\right] \\
& + E_0 \cdot J_5(m) \cdot \cos\left[(\omega_0 - 5\omega_{RF})t\right] \\
& + E_0 \cdot J_5(m) \cdot \cos\left[(\omega_0 + 5\omega_{RF})t\right]
\end{aligned}
$$

(19)

5.3 Theoretical calculations and simulation results

5.3.1   mm-Wave Signal Generation Based on The Proposed System

Here, we present a theoretical basis of the proposed mm-wave generation and transmission system. The concept behind the generation of the 60-GHz wireless signal is shown in Fig. 4-6, where only one single-electrode MZM is utilized. The optical field at the input of the single-electrode MZM is given by $E_{in}(t) = E_o \cos(\omega_c t)$, where E_o and ω_c are the amplitude and angular frequency of the optical field, respectively. The driving RF signal $V(t)$ consisting of two sinusoidal signals at different frequencies MZM is $V(t) = V_1 \cdot \cos \omega_1 t + V_2 \cdot \cos \omega_2 t$, where V_1 and V_2 are the signal amplitudes at frequency ω_1 and ω_2, respectively. To simplify the analysis, the power splitting ratio of the MZM is set as 0.5. In order to suppress the undesired optical carrier, the single-electrode MZM is biased at the null point. The optical field at the output of the MZM is then given by

$$E_{out}(t) = E_o \cdot \cos \omega_c t \cdot \cos[(\pi/2V_\pi) \cdot (V_\pi + V_1 \cdot \cos \omega_1 t + V_2 \cdot \cos \omega_2 t)]. \qquad (6)$$

Using Bessel function expansion, the output optical field at the output of the MZM can be rewritten as

$$
\begin{aligned}
E_{out}(t) = E_o \cdot \{ & J_0(m_2)J_1(m_1) \cdot \cos[(\omega_c \pm \omega_1)t] \\
& - J_0(m_2)J_3(m_1) \cdot \cos[(\omega_c \pm 3\omega_1)t] \\
& - J_1(m_1)J_2(m_2) \cdot \cos[(\omega_c + \omega_1 \pm 2\omega_2)t] \\
& - J_1(m_1)J_2(m_2) \cdot \cos[(\omega_c - \omega_1 \pm 2\omega_2)t] \\
& + J_0(m_1)J_1(m_2) \cdot \cos[(\omega_c \pm \omega_2)t] \\
& - J_0(m_1)J_3(m_2) \cdot \cos[(\omega_c \pm 3\omega_2)t] \\
& - J_1(m_2)J_2(m_1) \cdot \cos[(\omega_c + \omega_2 \pm 2\omega_1)t] \\
& - J_1(m_2)J_2(m_1) \cdot \cos[(\omega_c - \omega_2 \pm 2\omega_1)t] + ... \},
\end{aligned}
$$

(7)

where m_1 and m_2 are the modulation indices defined as $V_1\pi/2V_\pi$ and $V_2\pi/2V_\pi$, respectively. $J_n()$ is the n_{th} order Bessel function of the first kind. For a small modulation index the magnitude of Bessel function of the first kind is proportional to the order of the function. As shown in the Fig. 5-3, when the modulation index is small, the output optical field can be further simplified to

$$E_{out}(t) = E_o \cdot \{J_0(m_2)J_1(m_1) \cdot \cos[(\omega_c \pm \omega_1)t] + J_0(m_1)J_1(m_2) \cdot \cos[(\omega_c \pm \omega_2)t]\}. \tag{8}$$

After square-law photo detection the photocurrent of the mm-wave at frequency of $\omega_1 + \omega_2$ can be expressed as

$$i_{\omega_1+\omega_2} = R \cdot E_o^2 J_0(m_1)J_0(m_2)J_1(m_1)J_1(m_2), \tag{9}$$
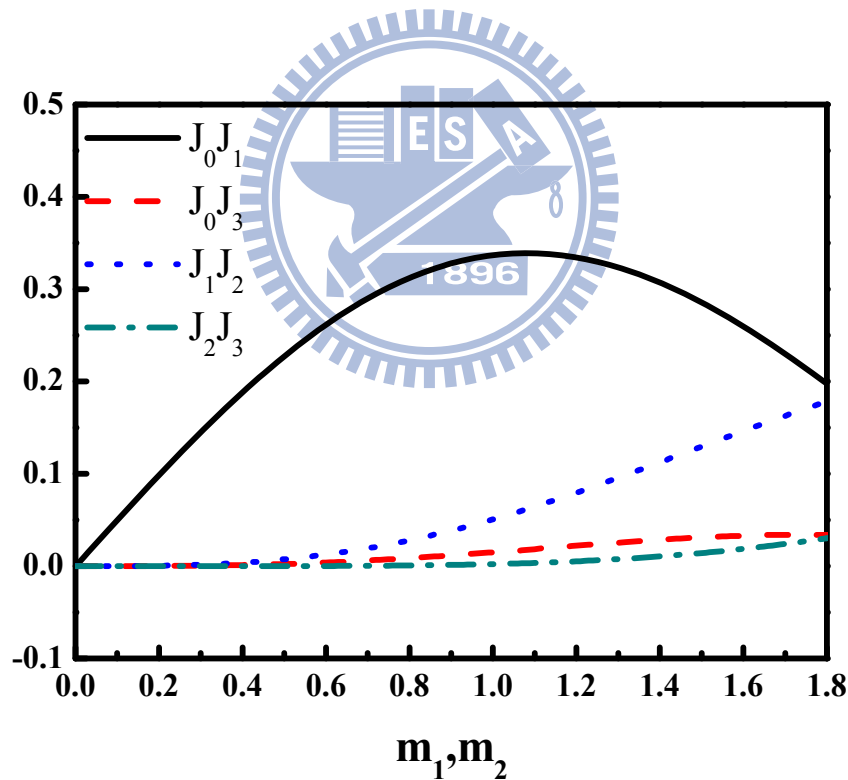
where R is the respresivity of photodiode.

Figure 5-3 The magnitude of Bessel functions versus different RF modulation index.

5.3.2 Dispersion Induce RF Fading Analysis and Beat Noise

When optical RF signals are transmitted over a standard single-mode fiber with dispersion, a phase shift to each optical sideband relative to optical carrier is induced by fiber dispersion. The propagation constant of fiber can be expressed as [29]

$$\beta(\omega) = n(\omega)\frac{\omega}{c} = \beta_0 + \beta_1(\omega - \omega_c) + \frac{1}{2}\beta_2(\omega - \omega_c)^2 + \cdots, \qquad (10)$$

where $\beta_m = (d^m\beta/d\omega^m)\big|_{\omega=\omega_c}$ is the derivative of the propagation constant evaluated at $\omega = \omega_c$. To simplify the analysis, the effect of high order fiber dispersion (i.e. 3rd order and higher) at 1550-nm band is neglected. For carrier tones with central frequency at $\omega = \omega_c \pm n\omega_{RF}$, we have $\beta(\omega_c \pm n\omega_{RF}) \cong \beta_0 \pm n\beta_1(\omega_c)\omega_{RF} + \frac{1}{2}n^2\beta_2(\omega_c)\omega_{RF}^2$ and, $\beta_2(\omega_c) = -(c/2\pi f_c^2)\cdot D(\omega_c)$ where c is light speed in free space, D is the chromatic dispersion parameter, and f_c is the frequency of the optical carrier. For a standard single-mode fiber, D is 17-ps/(nm.km). Therefore, after transmission over a standard single-mode fiber of length z, the electrical field can be written as

$$
\begin{aligned}
E_{OUT}(t) = E_o \cdot \{ & J_0(m_2)J_1(m_1)\cdot\cos[(\omega_c \pm \omega_1)t - \beta_0 z \mp \beta_1\omega_1 z - \tfrac{1}{2}\beta_2\omega_1^2 z] \\
+ & J_0(m_1)J_1(m_2)\cdot\cos[(\omega_c \pm \omega_2)t - \beta_0 z \mp \beta_1\omega_2 z - \tfrac{1}{2}\beta_2\omega_2^2 z] \}.
\end{aligned}
\qquad (11)
$$

After square-law photo detection, the photocurrent at the frequency of can be expressed as

$$i_{\omega_1+\omega_2}(t) = R \cdot E_o^2 J_0(m_1)J_0(m_2)J_1(m_1)J_1(m_2)\cdot\cos[\frac{1}{2}\beta_2 z(\omega_2^2 - \omega_1^2)]. \quad (12)$$

Due to fiber dispersion effect, the RF fading issue would be observed. The RF signal power is related to $\cos[\frac{1}{2}\beta_2 z(\omega_2^2 - \omega_1^2)]$. Therefore, the RF fading issue would become serious when the magnitude of sum frequency ($f_2 + f_1$) and

frequency difference ($f_2 - f_1$) become large.
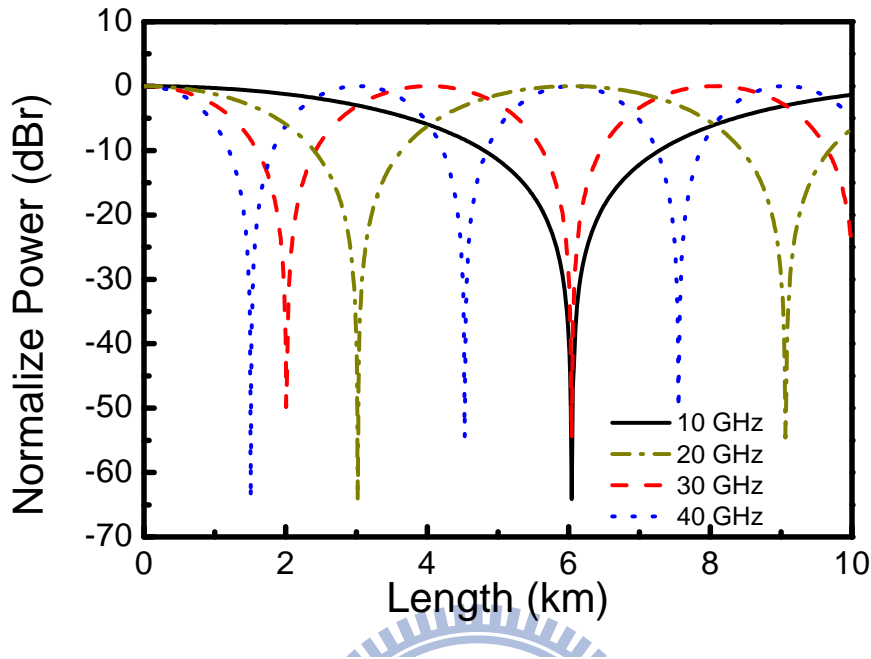
Figure 5-4 Simulated RF power of the generated mm-wave signal versus standard single-mode fiber length for various input frequency differences (i.e.

$f_2 - f_1$)

For 60-GHz applications, the sum frequency ($f_2 + f_1$) is fixed at 60.5 GHz, and the frequency difference ($f_2 - f_1$) will dictate the performance of RF fading. As shown in the Fig. 5-4, when the frequency difference increases, the RF power will drop off rapidly. For frequency differences of 10 GHz and 40 GHz, the first deep appears following 6 and 1.6-km fiber transmission, respectively. Not only does the smaller frequency difference result in a longer fiber transmission distance, but it also reduces the bandwidth requirements of the transmitter. However, the drawback of a small frequency difference is the risk of having beat noise interference. For example, if we choose 5.5 GHz as the frequency difference, and set the input frequencies at ω_2=33 GHz and ω_1=27.5

GHz, then with 7-GHz signal bandwidth, the generated signal will occupy frequencies from 24 to 31 GHz. As a result the beat noise (i.e. USB1 × LSB1) will fill the band from 48 to 62 GHz. Since the generated signal will fill the band from 57 to 64 GHz, the beat noise will fall in-band as shown in Fig. 5-5 (a), resulting in the possibility for severe system performance degradation. It is therefore necessary to choose proper frequencies of the input signals in the design process in order to avoid beat-noise induced system performance degradation. A good example is shown in Fig. 5-5 (b), where a frequency difference of 15.5 GHz is chosen, resulting in the beat noise occupying the band from 38 to 52 GHz and causing no interference.
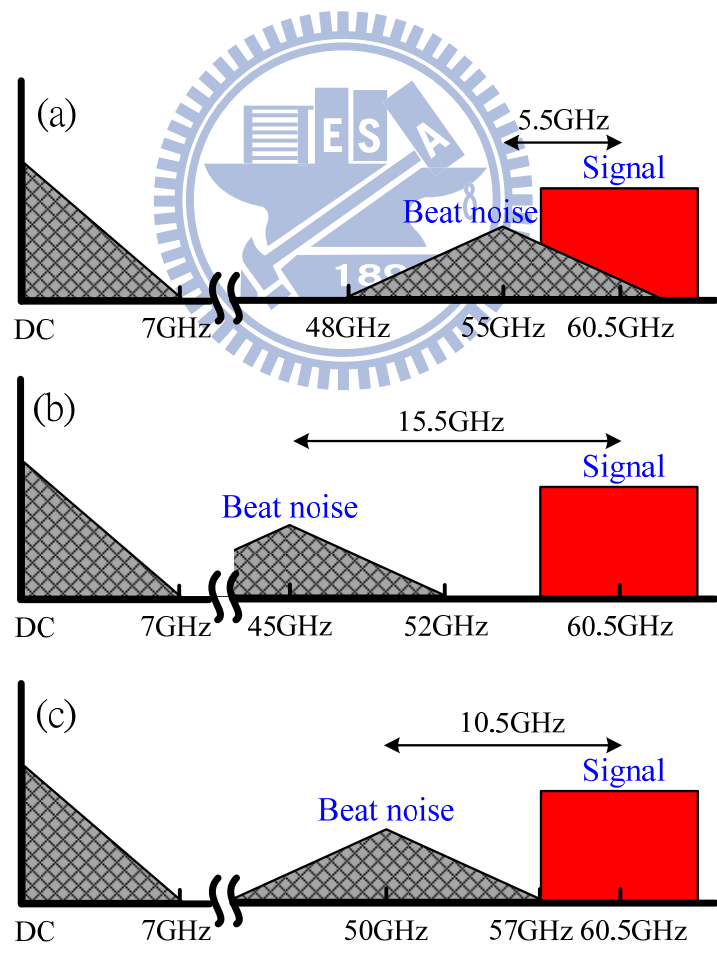

Figure 5-5 Beat noise interference in the proposed system and how to keep it from degrading system performance: (a) beat signal falls inside the desired band,

(b) beat signal is far away from desired band, and (c) beat noise is just outside the desired frequency band.

Therefore, there are tradeoffs between RF fading and beat noise interference. In the following analysis, we will choose the lowest possible frequency difference without causing any beat noise interference. With a target signal bandwidth of 7 GHz and center frequency of 60.5 GHz, we have

$$\begin{cases} f_1 + f_2 = 60.5 \text{ GHz} \\ 2(f_1 + 3.5) = 60.5 - 3.5 = 57 \text{ GHz} \end{cases} \tag{13}$$

This leads to a frequency difference equal to 10.5 GHz and input signal frequencies f_1=25 GHz and f_2=35.5 GHz, respectively. In this case the beat noise falls just outside the desired signal band, as shown in Fig. 5-5 (c). With the chosen frequency parameters, we can calculate the RF fading performance. Figure 5-6 (a) shows the RF power of the mm-wave signals generated between 57-64 GHz plotted against frequency. The line and circle represent theoretical results obtained using the model in equation (12) and VPI WDM-TransmissionMaker simulation results, respectively. It can be seen that RF fading is negligible over the whole 7-GHz spectrum for fiber spans up to 1 km. Beyond 1 km, frequencies in the lower part of the spectrum begin to experience increasing attenuation because they are generated from larger frequency differences. After 4 km of fiber transmission, the attenuation increases to 14 dB at 57 GHz and only 3 dB at 64 GHz. Nonetheless, for typical indoor applications, 2 to 3 km is more than enough [30]. On the other hand, if longer fiber transmission distances are needed, then any one of the four optical sidebands (see Fig. 4-6) may be filtered off to eliminate fading. To

compare the fading length of the proposed system to that of a DSB intensity-modulation direct detection (IMDD) transmission system, we plot the calculated and the simulated (VPI WDM-TransmissionMaker) fading (signal power) as a function of frequency. As Fig. 5-6 (b) shows, the first deep (total fading) at 60.5 GHz occurs after just 1 km of standard single-mode fiber transmission in the case of the DSB IMDD RoF system. Therefore, compared with the DSB IMDD RoF system, the proposed system offers superior transmission performance and more flexible system design.
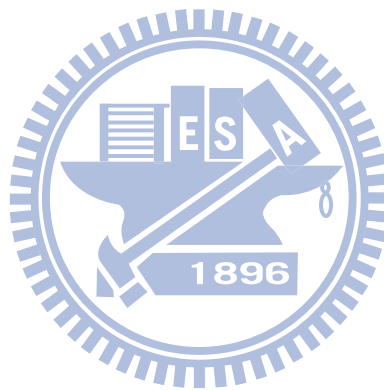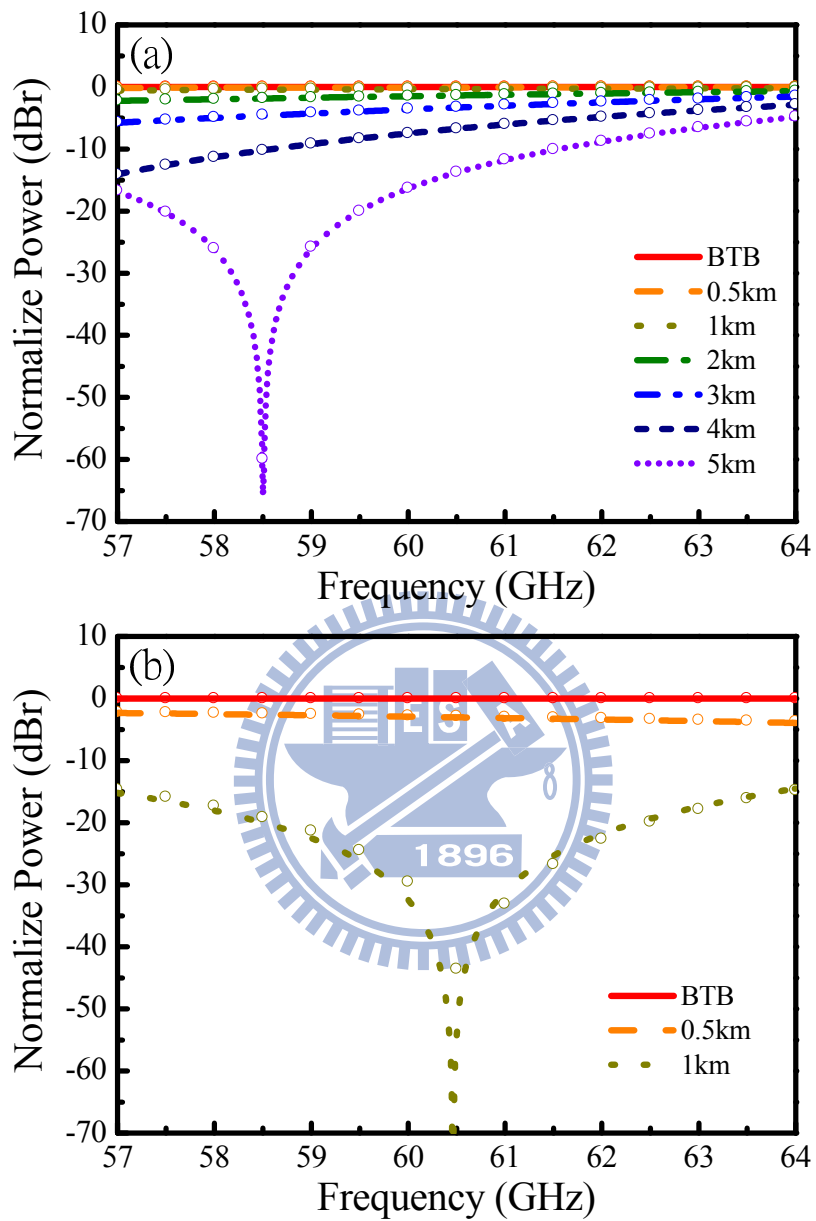
Figure 5-6 Simulations results of RF fading at 60 GHZ band versus different

transmission length, (a) proposed system, (b) double side band modulation

format.

Chapter 6

Experimental Demonstration of Proposed System

6.1 Preface

In this paper we propose a simple RoF system architecture for transporting and generating wideband single carrier signal at 60 GHz, and investigate its performance theoretically and experimentally. The RoF system uses only one single-electrode Mach-Zehnder modulator (MZM) having no more than 35.5-GHz bandwidth. We experimentally demonstrate the successful use of the simple RoF system to deliver a 13.875-Gb/s wireless signal at 60 GHz. The signal occupied the full 7-GHz spectrum at the 60-GHz band and used quadrature phase-shift keying (QPSK) modulation. Remote frequency up-conversion from the intermediate frequency (IF) to 60 GHz was achieved by employing a system configuration that used a 35.5-GHz local oscillator (LO) signal, which was transported alongside the signal. This enabled high-quality signal transmission over extended fiber lengths exceeding 3 km without any fiber dispersion compensation. The RoF link included a wireless transmission distance of 3 m.
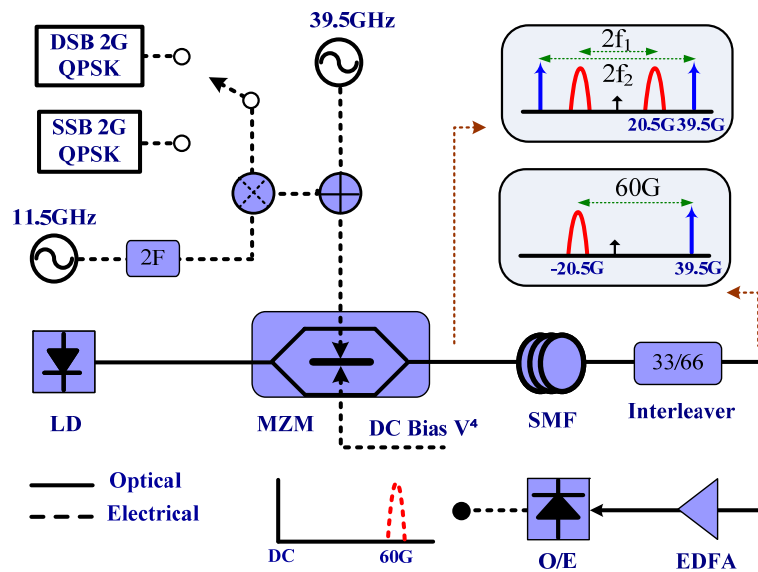
6.2 Experiment setup

Figure 6-1 The proposed RoF system based on a single-electrode MZM.

Fig.6-1 displays the experimental setup for optical vector signal generation and transmission using a single-drive modulator. The continuous wave (CW) laser is generated using a tunable laser with a central wavelength of 1550 nm. The RF signals are 2 GHz QPSK single sideband (SSB) and double sideband (DSB) signals. Besides, these two kinds of RF signals are up-converted using a two-tone 20.5 GHz (f1) and 39.5 GHz (f2) sinusoidal signals. At the remote node, a 33/66 interleaver removes the LSB2 and USB1. After the photo receiver, the optical signal generates RF signals with a difference frequency of 60 GHz (f1+f2). Additionally, the optical intensity of the data-modulated subcarriers (11.5 GHz) relative to that of the sinusoidal subcarrier (39.5 GHz) can be easily tuned by adjusting the input electrical power to optimize the performance of the optical RF signals. Furthermore, a frequency multiplication scheme is adopted to reduce the cost of the electronic components, especially for RF signals in the millimeter-wave range.

6.3 Experimental results

6.3.1 RF signal at different Carrier to Signal Ratio (CSR)

Fig. 6-2 and Fig. 6-3 show the optical spectrums and the BER curve in different SOPR (SOPR= P_s/P_d, P_s and P_d are the optical powers of the <u>35.5-GHz</u> subcarrier and the 25<u>-GHz </u>data-modulated subcarrier, respectively.) for DSB and SSB signal.
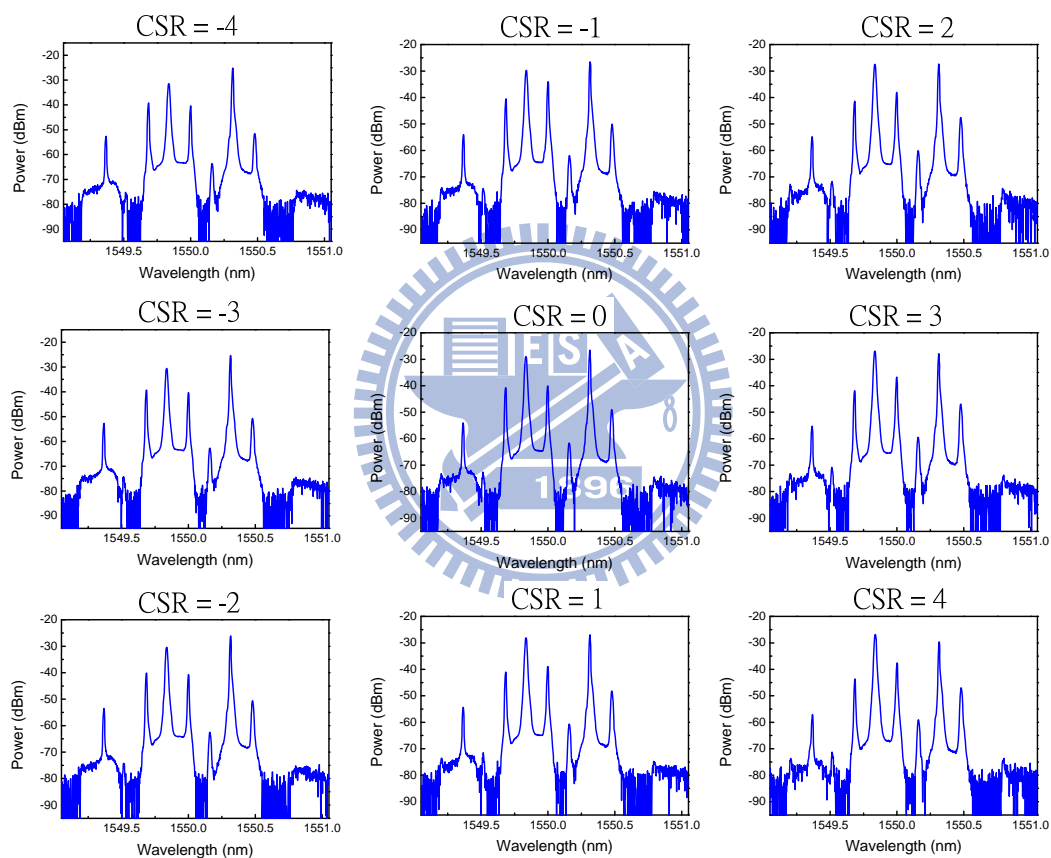
Figure 6-2 Optical spectrum for different CSR
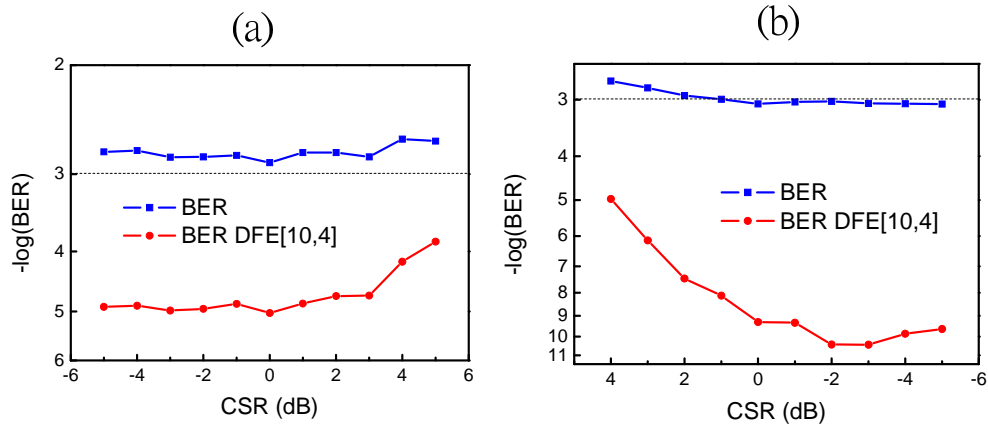
Figure 6-3 BER curve for different CSR (a) DSB (b) SSB

6.3.2 RF signal at different modulation index

In chaper5, the theoretical calculations results showed that the modulation index ($MI=V_{p-p}/2V_{\pi}$, V_{p-p} is the peak-to-peak voltage of the MZM driving signal) for driving MZM increases, the optical power ratio and electrical power ratio will be reduce. We also demonstrated experimental results for the different modulation index for driving MZM. Fig. 6-4 shows the optical spectrum before and after interleaver. Fig. 6-5 shows the MZM driving RF PSK signal at different modulation index when the LSB2 and USB1 is filtering.
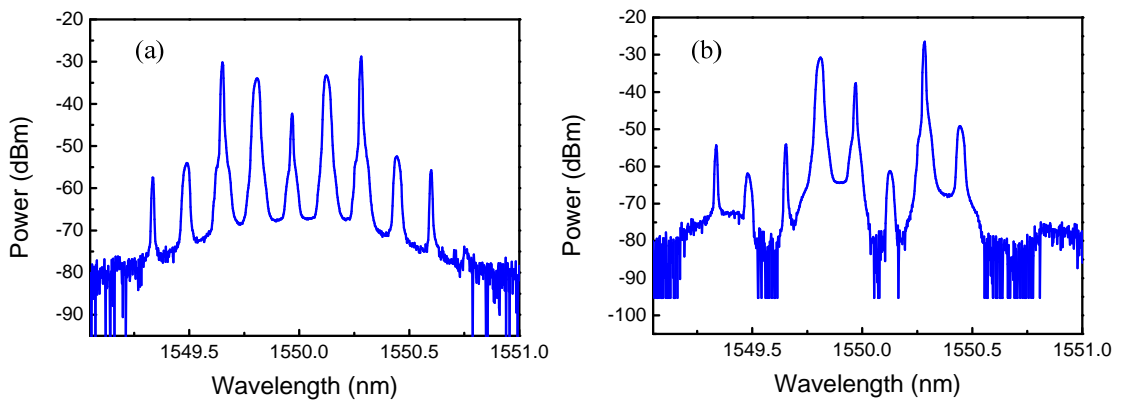
Figure 6-4 shows the optical spectrum before (a) and after (b) interleaver
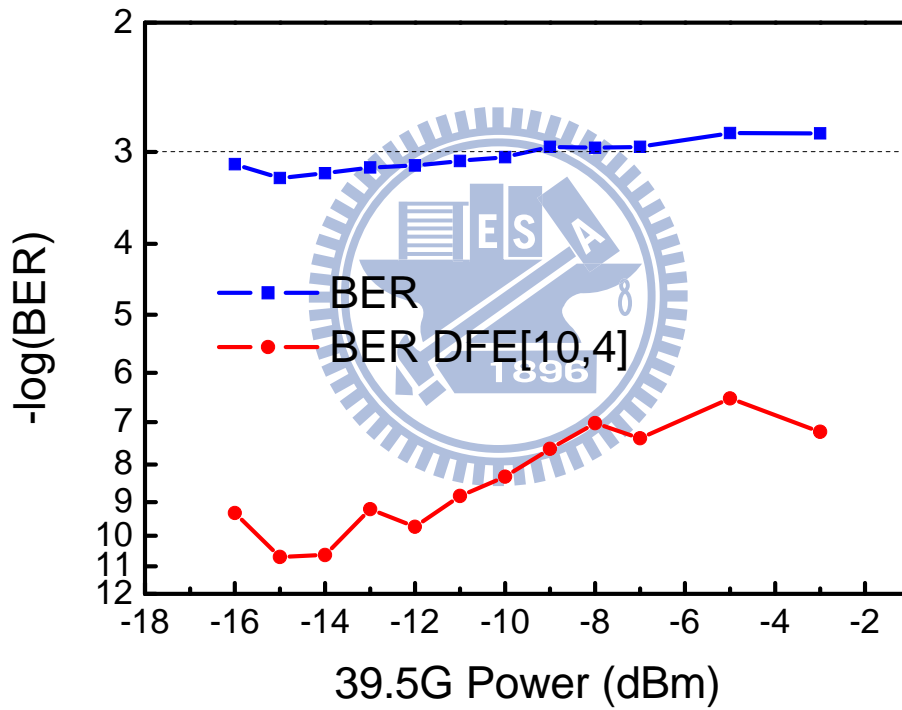
Figure 6-5 shows the signal performances at different modulation index

6.3.3 Transmission results
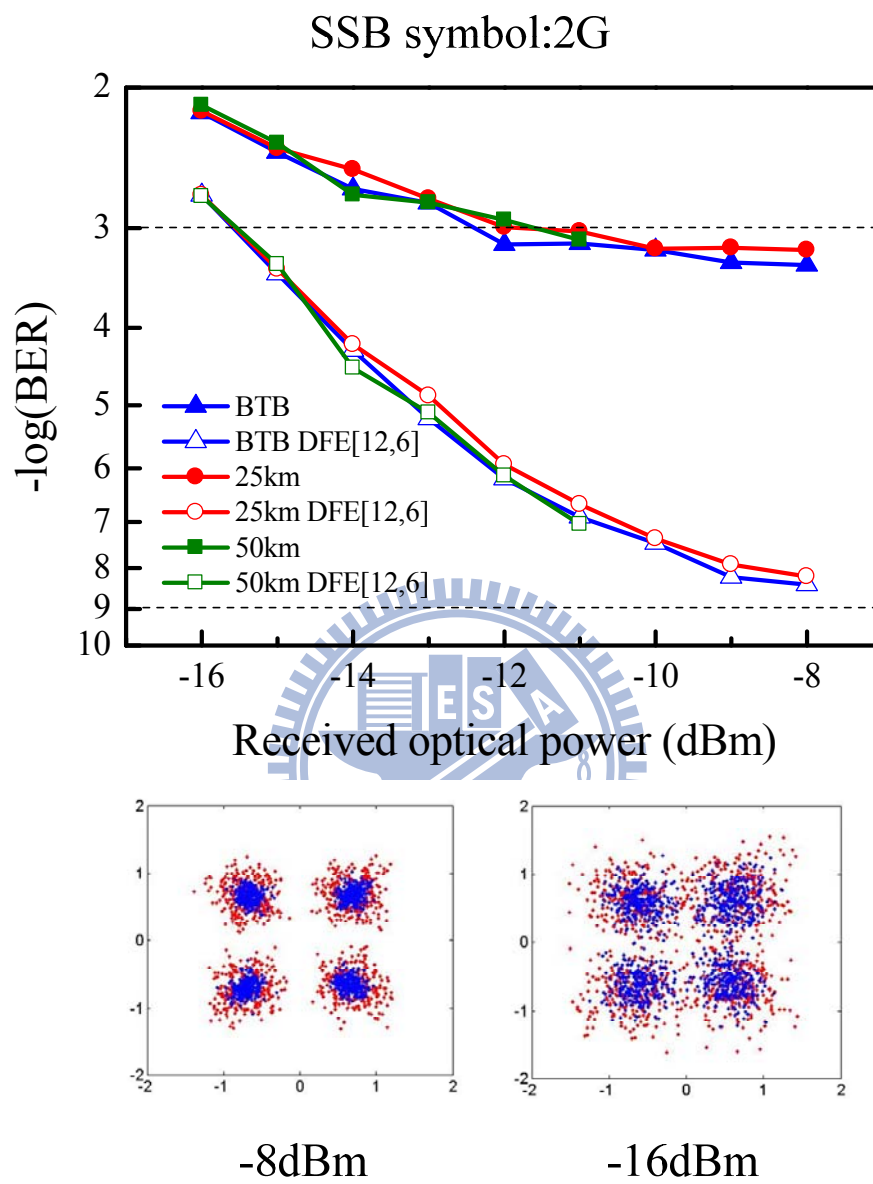
Figure 6-6 Single sideband signal BER curve and constellation for different

optical received power

DSB symbol:2G

-5dBm   -16dBm
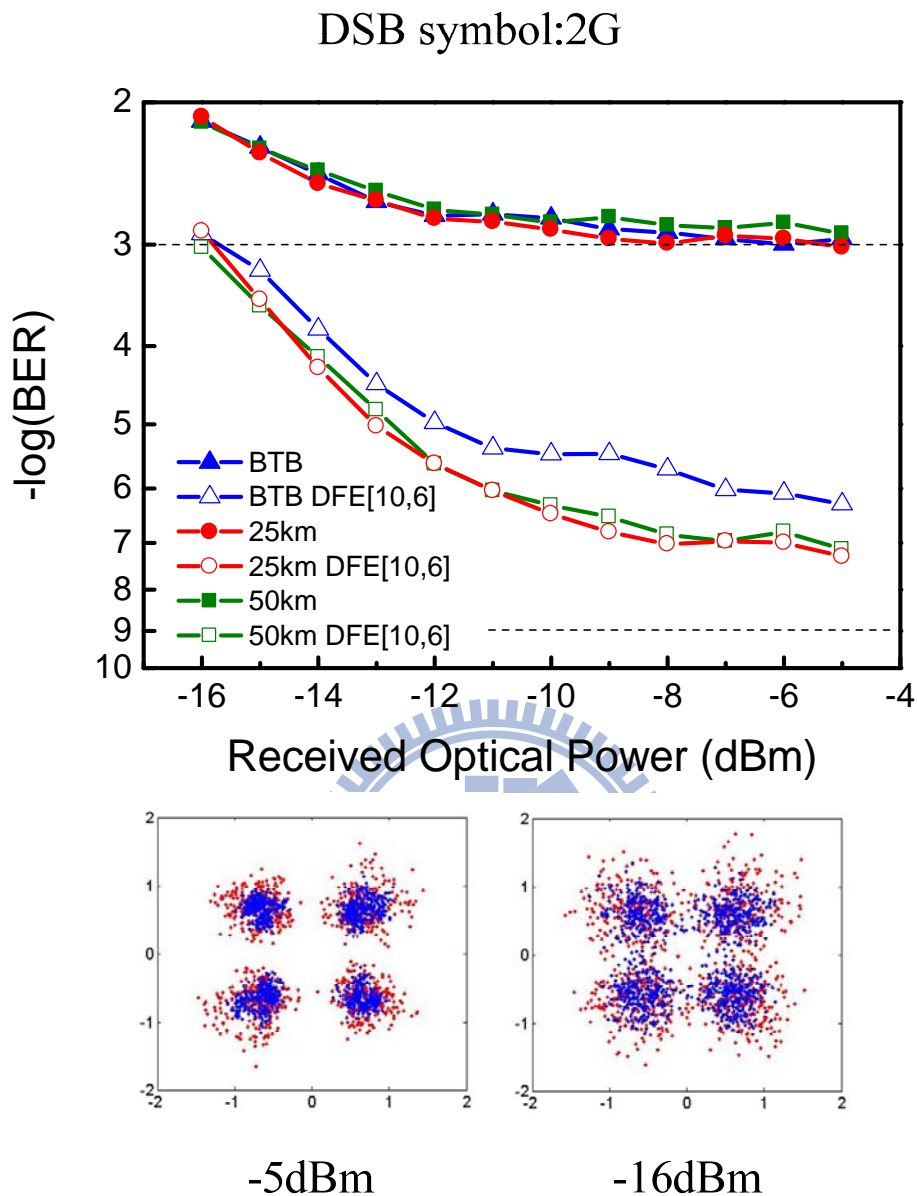
Figure 6-7 Double sideband signal BER curve and constellation for different

optical received power

In digital communications, an equalizer is a device that attempts to recover a

signal transmitted through an ISI channel. It may be a simple linear filter or a

complex algorithm. Here, we use a decision feedback equalizer (DFE) with

Least Mean Square (LMS) algorithm to recover the signal which is effect by

inter-symbol interference (ISI) channel and frequency response. The advantage of a DFE implementation is the feedback filter, which is additionally working to remove ISI, operates on noiseless quantized levels, and thus its output is free of channel noise.

Fig. 6-6 presents the measured receiver bit error rate (BER) curves of QPSK RF signals in different distances and before/after decision feedback equalizer (DFE) which has a ten taps feedforward taps and four feedback taps. After 25km and 50 km fiber transmission, there are only a few penalty (less than 1dB in BER), even after equalizer. Besides, there is a big improvement after an equalizer. The most improvement is about the power of four in BER. But there is only a small improvement about equalizer when input PD power is small. The reason is that the most influence is from noise which is random, so we can't use an equalizer to improve our signals.

Between the two figures, we can found that DSB signal is better than SSB signal about the power of two in BER. Because SSB signals interfere by ISI more significantly compare to DSB signals. The SSB signal has an even much smaller eye at the transmitter part, so an equalizer is necessary and helpful for this kind of SSB signal generation.

Chapter 7

Conclusion

We have theoretically and experimentally investigated the performance of a simple RoF system for transporting and generating multi-Gbps single-carrier-modulated wideband wireless signals at 60 GHz. The RoF system employs a single-electrode MZM and uses no linearization techniques. We also double the data throughput by employing Hilbert transform on the signal. Theoretical analysis of the proposed system shows that by choosing appropriate input signal frequencies, the system can achieve fiber transmission distances exceeding 50-km without any chromatic dispersion compensation after equalization. The theoretical analysis was confirmed by experimental results. The RoF system was successfully used to transport a 4-Gb/s single-carrier-modulated signal at 60 GHz over more than 50km of standard single-mode fiber. Experimental results showed that after 50km of fiber transmission equalizer can improve signal performance significantly and there was only a small optical power penalty at both BERs of 1×10^{-3} and 1×10^{-9}.

REFERENCES

[1] A. J. Lowery and J. Armstrong, "Orthogonal-frequency-division multiplexing for dispersion compensation of long-haul optical systems," Opt. Express 14, pp.2079-2084 (2006).

[2] I. B. Djordjevic and B. Vasic, "Orthogonal frequency division multiplexing for high-speed optical transmission," Opt. Express 14, pp.3767-3775 (2006).

[3] H. Bao and W. Shieh, "Transmission simulation of coherent optical OFDM signals in WDM systems," Opt. Express 15, pp. 4410-4418 (2007).

[4] W. H. Chen, and W. I. Way, "Multichannel Single-Sideband SCM/DWDM Transmission System," J. Lightwave Technol 22, pp.1697-1693 (2004).

[5] C. Wu, and X. Zhang, "Impact of Nonlinear Distortion in Radio Over Fiber Systems with Single-Sideband and Tandem Single-Sideband Subcarrier Modulations," J. Lightwave Technol. 24, pp.2076-2090 (2006).

[6] J. Yu, Z. Jia, L. Yi, G. K. Chang, and T. Wang, "Optical millimeter wave generation or up-conversion using external modulators," IEEE Photon. Technol. Lett. 18, pp.265–267 (2006).

[7] J. J. O'Reilly, P. M. Lane, R. Heidemann, and R. Hofstetter, "Optical generation of very narrow linewidth millimeter wave signals," Electron. Lett. 28, pp.2309–2311 (1992).

[8] C. Lim, M. Attygalle, A. Nirmalathas, D. Novak, and R. Waterhouse, "Analysis of Optical Carrier-to-Sideband Ratio for Improving Transmission Performance in Fiber-Radio Links," IEEE Trans. Microwave Theory Technol. 54, pp.2181-2187 (2006).

[9] L. N. Langey, M. D. Elkin, C. Edge, M. J. Wale, U. Gliese, X. Huang, and A. J. Seeds, "Packaged semiconductor laser optical phase-locked loop (OPLL) for photonic generation, processing and transmission of microwave signals," IEEE Trans. Microwave Theory Technol. 47, pp.1257-1264 (1999).

[10] C. S. Choi, Y. Shoji, and H. Ogawa, "Millimeter-wave fiber-fed wireless access system based on dense wavelength-division-multiplexing networks," IEEE Trans. Microwave Theory Technol. 56, pp.232-241 (2008).

[11] J. Wells, "Faster than fiber: the future of multi-Gb/s wireless," IEEE Microwave Magn. New York, vol. 10, pp. 104 – 112, May 2009.

[12] P. F. M. Smulders, "60 GHZ radio: Prospects and future directions," in Proc. IEEE Benelux Chapter on Communications and Vehicular Technology, Eindhoven, The Netherlands, 2003, pp. 1–8.

[13] R. Emrick, S. Franson, J. Holmes, B. Bosco, and S. Rockwell, "Technology for emerging commercial applications at millimeter-wave frequencies," in Proc. IEEE/ACES Int. Conf. Wireless Communications and Applied Computational Electromagnetics, 2005, pp. 425–429.

[14] B. Razavi, "Gadgets gab at 60 GHZ," IEEE Spectrum, vol. 45, no. 2, pp. 46-58, Feb 2008.

[15] C. Park, and T. S. Rappaport, "Short-range wireless communications for Next-Generation Networks: UWB, 60 GHZ millimeter-wave WPAN, and ZigBee," IEEE Wireless Communications, vol. 14, no.4, pp. 70-78, 2007.

[16] P. Smulders, "Exploiting the 60 GHZ band for local wireless multimedia access: prospects and future directions," IEEE Comm. Magn., vol. 40, no. 1, pp. 140-146, 2002.

[17] M. Sauer, A. Kobyakov, J. George, "Radio over fiber for picocellular network architectures," J. Lightw. Technol., vol. 25, no. 11, pp. 3301-3320, 2007.

[18] J. Yu, Z. Jia, L. Yi, Y. Su, T. Wang, G. K. Chang, and T. Wang, "Optical Millimeter-Wave Generation or Up-conversion Using External Modulators", IEEE Photon. Technol. Lett., Vol. 18, No. 1, pp. 265-267, Jan. 1, 2006.

[19] Z. Jia, J. Yu, A. Chowdhury, G. Ellinas, G. K. Chang, "Simultaneous Generation of Independent Wired and Wireless Services Using a Single Modulator in Millimeter-Wave-Band Radio-Over-Fiber Systems", IEEE Photon. Technol. Lett., Vol. 19, No. 20, pp. 1691–1693, Oct. 15, 2007

[20] A. M. J. Koonen, and M. García Larrodé, "Radio-Over-MMF Techniques—Part II: Microwave to Millimeter-Wave Systems," J. Lightw. Technol., Vol. 26, no. 15, pp. 2396–2408, Aug. 1, 2008.

[21] A. Ng'oma, M. Sauer, F. Annunziata, W. J. Jiang, C. T. Lin, J. Chen, P. T. Shi, and S. Chi, "Simple Multi-Gbps 60 GHZ Radio-over-Fiber Links Employing Optical and Electrical Data Up-conversion and Feed-Forward Equalization," in Proc. of Optical Fiber Communication Conf. 2009, San Diego, OWF2, Mar. 2009.

[22] M. Weiß, M. Huchard, A. Stöhr, B. Charbonnier, S. Fedderwitz, and D. S. Jäger, "60 GHZ photonic millimeter-wave link for short- to mediumrange wireless transmission up to 12.5 Gb/s," J. Lightw. Technol., vol. 26, no. 15, pp. 2424–2429, Aug. 1, 2008.

[23] Gen-ichiro OHTA, Mitsuru UESUGI, Takuro SATO, Members, and Hideyoshi TOMINAGA, Fellow, "Study of Orthogonal SSB Modulation Method," IEICE TRANS. FUNDAMENTALS, Vol.E87–A, No.10 Oct. 2004.

[24] John G. Proakis, Digital Communications, McGraw-Hill Companies, Inc., International Edition, 2001.

[25] Edward A. Lee, David G. Messerschmitt, Digital Communication, Kluwer Academic Publishers, Boston, 1988.

[26] Simon Haykin, Adaptive Filter Theory, Prentice-Hall, Inc., 1996.

[27] M. E. Austin, "Decision Feedback Equalization for Digital Communication Over Dispersive Channels", M.I.T. Research Laboratory of Electronics Technical Report 461, August 1967.

[28] M. KaveHrad and E. Savov, "Fiber-Optic Transmission of Microwave 64-QAM Signals," IEEE J. Sel. Areas in Commun. 8, pp.1320-1326 (1990).

[29] G. P. Agrawal, Fiber Optic Communication Systems, 3rd ed. New York: John Wiley & Sons, 2002.

[30] A. Flatman, "In-premises optical fibre installed base analysis to 2007.", IEEE 802.3 Gigabit Ethernet over FDDI-Grade Fiber Study group, Orlando, FL, USA, 2004.

Publication

1. Chun-Ting Lin, Po-Tsung Shih, Jason (Jyehong) Chen, Wen-Jr Jiang,,Sheng-Peng Dai, Peng-Chun Peng, <u>Yen-Lin Ho</u>, and Sien Chi, "Optical Millimeter-Wave Up-Conversion Employing Frequency Quadrupling Without Optical Filtering," ***IEEE TRANSACTIONS ON MICROWAVE THEORY AND TECHNIQUES***, VOL. 57, NO. 8, AUGUST 2009

2. F.-M. Kuo, <u>Yen-Lin Ho</u>, J.-W. Shi, Nan-Wei Chen, Wen-Jr Jiang, Chun-Ting Lin, Jason (Jyehong) Chen, Ci-Ling Pan and Sien Chi, "12.5-Gb/s Wireless Data Transmission by Using Bias Modulation of NBUTC-PD Based W-Band Photonic Transmitter-Mixer" **,** ***Optical Fiber Communication Conference and Exposition (OFC) 2010***

3. <u>Y. L. Ho</u>, C. T. Lin, P. T. Shih, W. J. Jiang, Jason(Jyehong) Chen, F. M. Kuo, N. W. Chen, J. W. Shi, S. Chi, "Generate and Transmiss W-band 3.75-Gb/s 8PSK Wireless Signal via Optical Frequency Octupling and Bias Modulation of NBUTC-PD with Feed-Forward Equalizer"**,** ***Optics And Photonics Taiwan (OPT) 2009***